AGU PUBLICATIONS

JGR

Journal of Geophysical Research: Atmospheres

RESEARCH ARTICLE
10.1002/2014JD022337

Key Points:
- The CMIP5 models provide a good simulation of TOA CREs but not clouds
- The ENSO effects in the CMIP5 models are affected by model biases in climatology
- The CMIP5 models show a large diversity in representing tropical cloud processes

Correspondence to:
H. Wang,
Hailan.Wang@nasa.gov

Citation:
Wang, H., and W. Su (2015), The ENSO effects on tropical clouds and top-of-atmosphere cloud radiative effects in CMIP5 models, *J. Geophys. Res. Atmos.*, *120*, 4443–4465, doi:10.1002/2014JD022337.

Received 18 JUL 2014
Accepted 20 APR 2015
Accepted article online 23 APR 2015
Published online 18 MAY 2015

The ENSO effects on tropical clouds and top-of-atmosphere cloud radiative effects in CMIP5 models

Hailan Wang[1,2] and Wenying Su[1]

[1]Climate Science Branch, NASA Langley Research Center, Hampton, Virginia, USA, [2]Science Systems and Applications, Inc., Hampton, Virginia, USA

Abstract The El Niño–Southern Oscillation (ENSO) effects on tropical clouds and top-of-atmosphere (TOA) cloud radiative effects (CREs) in Coupled Model Intercomparison Project Phase 5 (CMIP5) models are evaluated using satellite-based observations and International Satellite Cloud Climatology Project satellite simulator output. Climatologically, most CMIP5 models produce considerably less total cloud amount with higher cloud top and notably larger reflectivity than observations in tropical Indo-Pacific (60°E-200°E; 10°S-10°N). During ENSO, most CMIP5 models strongly underestimate TOA CRE and cloud changes over western tropical Pacific. Over central tropical Pacific, while the multi-model mean resembles observations in TOA CRE and cloud amount anomalies, it notably overestimates cloud top pressure (CTP) decreases; there are also substantial inter-model variations. The relative effects of changes in cloud properties, temperature, and humidity on TOA CRE anomalies during ENSO in the CMIP5 models are assessed using cloud radiative kernels. The CMIP5 models agree with observations in that their TOA shortwave CRE anomalies are primarily contributed by total cloud amount changes, and their TOA longwave CRE anomalies are mostly contributed by changes in both total cloud amount and CTP. The model biases in TOA CRE anomalies particularly the strong underestimations over western tropical Pacific are, however, mainly explained by model biases in CTP and cloud optical thickness (τ) changes. Despite the distinct model climatological cloud biases particularly in τ regime, the TOA CRE anomalies from total cloud amount changes are comparable between the CMIP5 models and observations, because of the strong compensations between model underestimation of TOA CRE anomalies from thin clouds and overestimation from medium and thick clouds.

1. Introduction

El Niño–Southern Oscillation (ENSO) is the leading mode of natural interannual climate variability in the tropical coupled ocean-atmosphere system. In the tropics, it considerably affects the Walker circulation and local Hadley circulation, and strongly perturbs tropical clouds and their radiative effects [*Cess et al.*, 2001a, 2001b; *Allan et al.*, 2002]. During the warm phase of ENSO (El Niño), the warmer sea surface temperature (SST) anomalies in the central and eastern tropical Pacific induce notable ascent over the central tropical Pacific, thereby stronger tropical deep convection and more high clouds, resulting in enhanced top-of-atmosphere (TOA) shortwave cooling and longwave warming anomalies there. Meanwhile, over the western tropical Pacific, the cooler SST anomalies lead to local anomalous subsidence, suppressed tropical deep convection, and reduced formation of high clouds, resulting in weakened TOA shortwave cooling and longwave warming effects. The opposite of the above occurs during the cold phase of ENSO (La Niña). The detailed ENSO effects on tropical clouds and TOA cloud radiative effects (CREs) vary considerably from event to event, as they depend on the spatial pattern and magnitude of SST anomalies associated with individual ENSO events [e.g., *Su and Jiang*, 2013]. The ENSO effects on tropical clouds and TOA radiative fluxes have been used as a test bed for evaluating climate models [e.g., *Cess et al.*, 2001b; *Sun et al.*, 2012].

General circulation model (GCM) simulations of ENSO and its atmospheric effects are strongly influenced by model mean state [e.g., *Guilyardi et al.*, 2009], particularly those of SST, precipitation, and atmospheric circulation. While GCMs simulate large-scale features of the above fields well, they are deficient in simulating many regional details [e.g., *Neelin et al.*, 1992; *Mechoso et al.*, 1995; *Latif et al.*, 2001; *Meehl et al.*, 2005]. One of the most outstanding GCM biases is a double intertropical convergence zone (ITCZ) pattern with excessive precipitation off the equator but insufficient precipitation on the equator. The recent Coupled Model Intercomparison Project (CMIP) Phase 5 (CMIP5) coupled GCMs (CGCMs) still exhibit significant double ITCZ biases with magnitude comparable to those in the CMIP Phase 3 (CMIP3) CGCMs

[*Li and Xie*, 2014]. Such model bias is associated with the biases in ocean-atmosphere feedback over the equatorial Pacific, including the excessive Bjerknes feedback, the overly positive SST-latent heat flux feedback, and the insufficient SST-shortwave flux feedback [*Lin*, 2007; *Lloyd et al*., 2011]. Part of the double ITCZ biases are also caused by the weak model deep convective sensitivity to environmental moisture which results in the deep convection being insufficiently suppressed and thus occurring over the dry subsidence region of the southeastern Pacific [*Nagio and Takayabu*, 2013]. The double ITCZ bias can originate from the Southern Hemisphere extratropics as well, as the cloud biases there can explain most of the inter-model differences in the amount of excessive precipitation in the Southern Hemisphere tropics [*Hwang and Frierson*, 2013; *Li and Xie*, 2014]. There is also excessive precipitation over the Northern Hemisphere (NH) western subtropical Pacific [*Liu et al*., 2012].

Another prominent mean bias in many GCMs is the underestimation of precipitation, deep convection, and high clouds over the Maritime Continent [e.g., *Wang and Su*, 2013], where the models are deficient in resolving the diurnal cycle and local geography over these tropical islands which can rectify onto the seasonal mean climate [*Neale and Slingo*, 2003]. In particular, the model diurnal cycle tends to peak too early in the day instead of in the late afternoon or evening as in the observations. Such model biases mainly originate from the deficiencies in model convective parameterization schemes rather than model resolution [*Sato et al*., 2009; *Dirmeyer et al*., 2012; *Pearson et al*., 2014]. Some improvements can be made by changing the parameterization schemes, particularly adjusting the dependence of entrainment rates on the surrounding atmospheric conditions [*Slingo et al*., 2004; *Wang et al*., 2007; *Del Genio and Wu*, 2010; *Stratton and Stirling*, 2012]. The dry bias over the Maritime Continent can further drive other systematic model errors, such as the excess precipitation over the western tropical Indian Ocean [*Neale and Slingo*, 2003].

The GCMs are deficient in simulating climatological clouds and their radiative effects as well [e.g., *Potter and Cess*, 2004; *Su et al*., 2010]. Owing to the development of satellite simulators and the availability of model satellite simulator output in recent years, the model clouds can be evaluated by directly comparing with the observations. The satellite simulator produces model clouds that a specific satellite would observe as if it were flying over the model atmosphere, thus increasing the chances that the differences of clouds between that model and the observations reflect the model biases. The evaluation of GCM clouds in the context of satellite simulator output [e.g., *Klein et al*., 2013] shows that GCMs have been simulating considerably less cloud amount with notably higher reflectivity. While the CMIP5 models have shown marked improvements over the CMIP3 models in simulating more cloud amounts with less reflectivity, the above model biases are still prominent. Recent studies [e.g., *Nam et al*., 2012; *Wang and Su*, 2013] also show that the CMIP5 models lack middle clouds and produce too few yet overly bright subtropical low stratocumulus clouds. While the CMIP5 models only moderately underestimate the tropical mean high cloud amount, they exhibit considerable regional biases by producing less high clouds over the Maritime Continent and more high clouds over the trade cumulus regions. The CMIP5 model errors in clouds are primarily attributable to the errors in the model cloud parameterizations, with the model errors in large-scale dynamical and thermodynamic fields playing secondary roles [*Su et al*., 2012].

Past studies on ENSO effects on tropical clouds and TOA CREs mainly focused on the observed processes by using satellite-based observations [e.g., *Cess et al*., 2001a, 2001b; *Lu et al*. 2004; *Sun et al*., 2012]. The evaluation of model simulations of this subject, particularly changes in cloud properties (cloud amount, cloud top altitude, and cloud optical thickness) and their relative quantitative roles in contributing to the TOA CRE anomalies during ENSO, has not been well addressed, mainly due to lack of satellite simulator output. Furthermore, limited by short temporal span of data used, past studies mainly focused on individual ENSO events; their findings thus may be specific to the ENSO event studied. Extending the work in *Cess et al*. [2001a, 2001b] and *Lu et al*. [2004], *Sun et al*. [2012] provide a comprehensive evaluation of a NCAR model simulation of cloud structure changes and their associated radiative property changes over the tropical Pacific Ocean during the strong 1997/98 El Niño. With a radiative transfer model and Clouds and the Earth's Radiant Energy System (CERES) observations, they were able to quantify the observed relative contribution of cloud fraction, cloud top height, cloud optical thickness, and temperature and specific humidity, to the TOA CRE anomalies during the 1997/98 El Niño event. They were, however, unable to do the same for the NCAR model for an apples-to-apples comparison, due to lack of the CERES like four-layer cloud properties in the model International Satellite Cloud Climatology Project (ISCCP) simulator output.

Recently, a number of AGCMs participating in the CMIP5 produced ISCCP [*Klein and Jakob*, 1999; *Webb et al*., 2001; *Pincus et al*., 2012; *Zhang et al*., 2012] satellite simulator output as a part of the Atmospheric Model Intercomparison Project (AMIP) simulations. The ISCCP satellite simulator provides the joint histogram of cloud top pressure (CTP) and cloud optical thickness (τ) for cloud fraction over multiple decades (July 1983 to June 2008), and thus is valuable for evaluating model simulations of cloud property changes associated with ENSO. Meanwhile, there have been significant advances in the development of methodologies to quantify the effects of clouds on TOA CREs. *Zelinka et al*. [2012a] introduced cloud radiative kernels which quantify the sensitivity of TOA radiative fluxes to cloud fraction perturbations within the framework of ISCCP joint CTP-τ histogram. Multiplying the cloud radiative kernels with changes in ISCCP cloud fraction element-wise between two climate states can provide a quantitative estimate of cloud-induced TOA radiation anomalies. Further, *Zelinka et al*. [2012b] developed a new methodology to quantify the relative roles of cloud property changes in contributing to TOA cloud-induced radiative flux anomalies. *Zelinka et al*. [2013] further improved the decomposition technique in *Zelinka et al*. [2012b] by considerably reducing the effects of a residual component and better isolating the relative TOA radiative effects of individual cloud properties. In this study, by leveraging the CMIP5 ISCCP satellite simulator output and following the methodologies developed by *Zelinka et al*. [2012a, 2012b, 2013], we perform a comprehensive evaluation of the CMIP5 model simulations of ENSO effects on tropical clouds and TOA CREs. This includes an assessment of the relative roles of changes in various cloud properties, as well as changes in temperature and humidity, in contributing to the TOA CRE anomalies during ENSO in the CMIP5 model simulations. A series of offline Fu-Liou radiative transfer calculations, including derivations of cloud radiative kernels, are performed to assess the CMIP5 simulations of the above processes.

This paper is organized as follows. Section 2 describes the data and methods. Section 3 evaluates the CMIP5 model simulations of TOA CREs and clouds in their climatologies and anomalies associated with ENSO over the tropical Indo-Pacific. Using cloud radiative kernels, section 3 also quantifies the relative roles of model cloud biases in various CTP-τ regimes in contributing to the model biases in TOA CRE anomalies during ENSO. Additionally, it assesses the CMIP5 model representation of the relative effects of changes in various cloud properties and changes in temperature and humidity on the TOA CRE anomalies. The summary and conclusions are given in section 4.

2. Data and Methods

2.1. Satellite-Based Observations and CMIP5 AMIP Simulations

The satellite-based observations used to evaluate the CMIP5 models include CERES Energy Balanced and Filled (EBAF) Edition 2.7 TOA radiative fluxes [*Loeb et al*., 2009] and the ISCCP joint CTP-τ histogram for cloud fraction [*Pincus et al*., 2012; *Zhang et al*., 2012].

The CERES EBAF TOA clear-sky and all-sky shortwave and longwave radiative fluxes are used to evaluate the TOA CREs in the CMIP5 AMIP simulations. The TOA solar insolation is based on daily varying Solar Radiation and Climate Experiment measurements and has a long-term mean of about 1361 W m^{-2}. The grid-box mean of clear-sky TOA fluxes from the EBAF Edition 2.7 are determined using an area-weighted average of CERES/Terra broadband fluxes from completely cloud-free CERES footprints (20 km equivalent diameter at nadir), and the Moderate Resolution Imaging Spectrometer (MODIS)/Terra-derived "broadband" clear-sky fluxes (1 km) estimated from the cloud-free portions of partly and mostly cloudy CERES footprints. With an objective constrainment algorithm, the all-sky shortwave and longwave fluxes are adjusted within their range of uncertainty to remove the inconsistency between global net TOA flux and heat storage in the Earth-atmosphere system. For the Terra-Aqua period (July 2002 to December 2010), the regional uncertainties in 1°×1° TOA all-sky shortwave and longwave fluxes are respectively 2.7 and 2.0 W m^{-2}, whereas the overall regional uncertainties for TOA clear-sky shortwave and longwave fluxes are respectively 2.6 and 3.6 W m^{-2}. These uncertainties are of one order smaller than the differences between the CERES observations and CMIP5 model simulations during individual months and thus do not affect our model evaluations. The EBAF TOA data are at a resolution of 1° latitude/longitude and are available monthly over the period March 2000 to October 2013.

The ISCCP joint CTP-τ histogram of cloud fraction is used to evaluate the CMIP5 model clouds. This product is derived from the ISCCP D1 data which are quasi-instantaneous spatial averages of pixel-level retrievals over

Table 1. List of the Seven CMIP5 AGCMs Analyzed in This Study

Model No.	Modeling Group	Model ID	Country	Atmospheric Resolution	Reference
1	CCCMA	CanAM4	Canada	2.8° × 2.8°	*von Salzen et al.* [2012]
2	CNRM	CNRM-CM5	France	1.4° × 1.4°	*Voldoire et al.* [2012]
3	NOAA GFDL	GFDL-CM3	USA	0.3° × 0.3°	*Delworth et al.* [2012]
4	Met Office Hadley Centre	HadGEM2-A	UK	1.9° × 1.3°	*Martin et al.* [2011]
5	AORI	MIROC5	Japan	1.4° × 1.4°	*Watanabe et al.* [2010]
6	Max Planck Institute for Meteorology	MPI-ESM-LR	Germany	1.9° × 1.9°	*Raddatz et al.* [2007]
7	MRI	MRI-CGCM3	Japan	1.1° × 1.1°	*Mizuta et al.* [2012]

equal-area grid cells [*Rossow and Schiffer*, 1999]. The CTP and τ bin edges for the ISCCP histogram are respectively 50, 180, 310, 440, 560, 680, 800, and 1100 hPa, and 0.3, 1.3, 3.6, 9.4, 23, 60, and 380. The data are at a horizontal resolution of 2.5° latitude/longitude and are available monthly over the period July 1983 to June 2008.

For the CMIP5 model evaluation, we analyze AMIP-style simulations from seven CMIP5 AGCMs that provide the ISCCP satellite simulator output (Table 1). The AMIP simulations are used because they are forced with observed monthly SST and sea ice fraction, and thus agree with the observations for the occurrence of ENSO events. Further, the AMIP experimental setup is well suited for studying atmospheric response to ENSO in the tropics where ocean plays an active role in forcing atmospheric changes [*Jha and Kumar*, 2009]. All the models except the CNRM-CM5 are forced with the combinations of most, if not all, of the following external forcing agents: well-mixed greenhouse gasses, black carbon, organic carbon, sea salt, mineral dust, anthropogenic sulfate aerosol direct and indirect effects, tropospheric and stratospheric ozone, land use change, solar irradiance, and volcanic aerosols. The CNRM-CM5 AMIP is forced with only greenhouse gasses and volcanic aerosol along with an 11 year solar cycle. The AMIP simulations are available monthly over the period January 1979 to December 2008.

The CTP and τ bin edges of model cloud fraction from the ISCCP satellite simulator output are respectively 50, 180, 310, 440, 560, 680, 800, and 1000 hPa, and 0, 0.3, 1.3, 3.6, 9.4, 23, 60, and 380. They are identical to those of the ISCCP observations, except some minor differences at the first and the last CTP and τ bins. Notably, compared with the observations, the ISCCP simulator histogram contains an additional optical depth bin for very thin clouds ($0 < \tau < 0.3$) that cannot be detected by the ISCCP passive sensors but can be "retrieved" by the ISCCP simulator. Despite these minor differences, the model data can be directly compared with the ISCCP observations for $\tau > 0.3$ bins (personal communications with Dr. Yuying Zhang, 2014). Thus, in this study, we only consider the CMIP5 ISCCP simulator output for $\tau > 0.3$ bins. In addition, following the cloud-type definitions used in the ISCCP D-series data sets [*Rossow and Schiffer*, 1999], the low, middle, and high clouds are referred to as clouds with CTP greater than 680 hPa, between 680 and 440 hPa, and less than 440 hPa, respectively; the thin, medium, and thick clouds are referred to as those with τ less than 3.6, between 3.6 and 23, and larger than 23, respectively.

While the ISCCP satellite simulator is meant to provide an apples-to-apples comparison between modeled and observed clouds, we need to use caution when interpreting differences within each CTP-τ bin of the histogram [*Klein et al.*, 2013]. Based on the comparisons with clouds retrieved from ground-based remote sensors that passed through the ISCCP simulator, *Mace et al.* [2011] suggest that the uncertainty of ISCCP retrievals is about ±200 hPa for CTP and a factor of 3 for τ. In addition, the large observational uncertainties for thin clouds suggest that differences with observations for bins of low τ may not reflect model errors. In this study, in addition to showing the results at the original 6 × 7 CTP-τ histogram in figures, we also display in tables aggregated results into a reduced-resolution joint histogram of CTP and τ with bin boundaries in CTP of 440 and 680 hPa and in τ of 3.6 and 23.

2.2. Analysis Methods

The model evaluations are performed by comparing observations with model simulations over periods that both data are available, i.e., 2001–2008 for TOA radiative fluxes and CREs, and 1984–2007 for all the results that are based on the ISCCP satellite simulator output. The use of different periods does not appreciably affect our main results and conclusions. For a field of interest, its anomaly associated with ENSO is obtained by linearly regressing its deseasonalized anomaly against the Multivariate ENSO Index (MEI)

[*Wolter and Timlin*, 2011] using least squares. Since this study focuses on general ENSO effect, data of all 12 months are used for the linear regression so as to increase the number of samples for more robust results. In addition, because this study focuses on statistics of model simulations, only one AMIP member from each of the models is used. To facilitate the comparison, all the AMIP simulations are regridded onto the spatial grids of the satellite-based observations via bilinear interpolation which has been shown to have minimal effect on the regional distribution [*Wang and Su*, 2013].

2.3. The Fu-Liou Radiative Transfer Model and Derivation of Cloud Radiative Kernels

The Fu-Liou radiative transfer model used in this study is based on the original Fu-Liou model [*Fu and Liou*, 1992] and is further developed at the NASA Langley Research Center [*Rose et al*., 2013]. The cloud radiative kernels are derived following *Zelinka et al*. [2012a], with several modifications made to better suit the subject of this study and the radiative transfer model we use.

For the observations and each of the seven CMIP5 models, we derive the cloud radiative kernels for each tropical 2.5° latitude-longitude grid and each calendar month, using their respective monthly climatologies over the period 1984–2007. The derivation of cloud radiative kernels at each tropical grid is necessary for this study, as it accounts for the zonal variations of TOA CRE sensitivity to cloud fraction perturbations, and thus can better quantify the effects of cloud changes on TOA CRE anomalies during ENSO. In the experiments for the observations, all the climatological input fields except surface albedo are averaged over 1984–2007 using NASA Modern Era Retrospective-Analysis for Research and Applications [*Rienecker et al*., 2011]. The surface albedo climatology is computed using 2001–2008 surface upwelling and downwelling shortwave fluxes from the CERES surface EBAF Edition 2.7 [*Kato et al*., 2013]. Note that the CERES surface EBAF Edition 2.7 data are only available for the period March 2000 onwards. It uses ocean spectral surface albedo from *Jin et al*. [2004] and broadband land surface albedos inferred from the clear-sky TOA albedo derived from CERES measurements [*Rutan et al*., 2009]. The use of 2001–2008 rather than 1984–2007 for surface albedo climatology should have little effect on the derived cloud radiative kernels in the tropical Indo-Pacific. In the Fu-Liou radiative transfer experiments for the CMIP5 models, all the input fields are taken from the models.

In addition, since this study mainly focuses on the tropical Indo-Pacific region, the aerosol radiative effect is minimized by setting the aerosol type as sea salt and the aerosol optical thickness at a rather small number (10^{-5}). Our test runs show that such aerosol setting yields negligible TOA CRE effects from aerosol; using sea salt optical thickness similar to that of the observed (0.1) leads to little difference in the cloud radiative kernels derived.

The shortwave and longwave cloud radiative kernels for each CTP-τ bin are obtained as the differences between TOA clear-sky and all-sky fluxes corresponding to 1% cloud fraction change. The time series of the joint CTP-τ histogram for the TOA CRE anomalies is subsequently computed by multiplying the time series of the deseasonalized ISCCP cloud fraction by the monthly cloud radiative kernels, element by element. The above time series of joint CTP-τ histogram of anomalous TOA CREs is then linearly regressed against the MEI to obtain the joint CTP-τ histogram of TOA CRE anomalies associated with ENSO. The above is performed for the observations and each of the seven CMIP5 models, using their respective cloud radiative kernels and ISCCP cloud fraction. We note that such kernel-derived TOA CRE anomalies are by design due solely to changes in clouds. For convenience, they are referred to as "cloud-induced TOA CREs" hereafter, to distinguish from the TOA CREs from noncloud processes, such as TOA radiation anomalies caused by temperature and humidity changes during ENSO [*Zhang et al*., 1994; *Soden et al*., 2004].

To assess the CMIP5 model representation of the relative roles of changes in cloud properties in contributing to the TOA CRE anomalies during ENSO, we follow the methodology in Appendix B of *Zelinka et al*. [2013] and decompose the cloud-induced TOA radiation anomalies into those due to total cloud amount changes, changes in CTP, changes in τ, and a residual term. We note that the total cloud amount changes refer to a hypothetical change in total cloud cover holding that fixed the cloud distribution across CTP and τ categories. See *Zelinka et al*. [2013] for more details of the decomposition methodology.

The effects of changes in temperature and specific humidity on TOA CRE anomalies during ENSO are also investigated. This is carried out by repeating the above calculations but using temperature and humidity that are the sum of their climatologies and anomalies due to ENSO when deriving cloud radiative kernels.

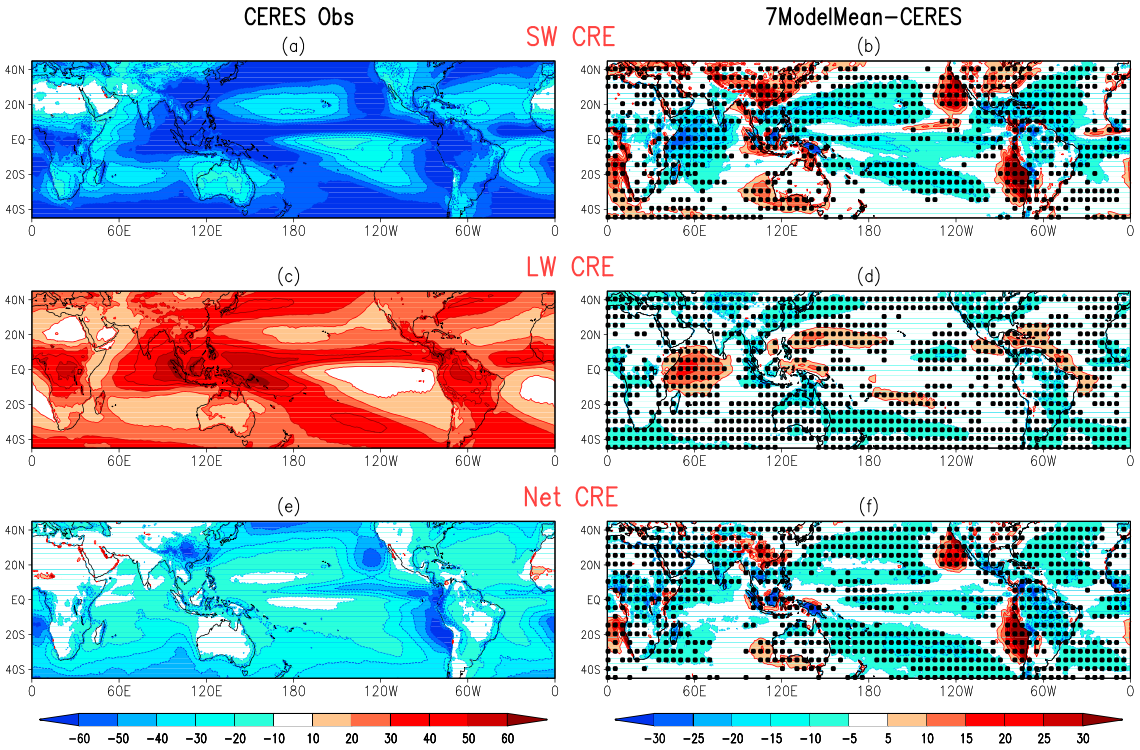

Figure 1. The annual mean climatology (2001–2008) of shortwave TOA CRE in (a) the CERES EBAF Edition 2.7 observations and (b) the CMIP5 7-model mean minus the CERES EBAF observations; Figures 1c and 1d show the same as Figures 1a and 1b except for longwave TOA CRE; Figures 1e and 1f show the same as Figures 1a and 1b except for net TOA CRE. Stippling indicates regions where at least five of the seven models agree with the 7-model mean in the sign of their biases. Units: W m^{-2}.

The differences between these two sets of calculations can then help quantify the effects of temperature and humidity changes on TOA CRE anomalies through changing TOA all-sky and clear-sky radiative fluxes. Note that such comparison provides a clean quantification of the effects of temperature and humidity changes on TOA clear-sky flux anomalies but only an approximation for TOA all-sky flux anomalies. This is because the cloud radiative kernels are by design based on monthly climatologies, rather than a state that contains ENSO anomalies. Given the rather small magnitude of cloud fraction anomalies in the CTP-τ bins as shown later (Figure 7), however, the results are presumably linear, and the above comparison should provide a rough estimation of the effects of temperature and humidity on TOA all-sky flux anomalies and hence TOA CRE anomalies.

Lastly, we note that the TOA CRE anomalies obtained using the above offline Fu-Liou radiative transfer calculations are not intended for a quantitative comparison with the TOA CREs produced by the CMIP5 models. This is not only because the kernel-derived TOA CREs are due solely to cloud changes but also because the CMIP5 models may use radiative transfer models that are quite different from the Fu-Liou model; they may also use varying assumptions and treatment of cloud processes when producing their TOA radiative fluxes.

3. Results

3.1. Climatology

Since the tropical mean state provides the background for atmospheric effects of ENSO, we first evaluate the CMIP5 model simulations of tropical TOA CRE and cloud climatologies. Figure 1 shows the annual climatologies of TOA shortwave, longwave, and net CREs in the CERES EBAF observations over the period 2001–2008 and the corresponding CMIP5 multi-model mean biases. The observations show distinct TOA shortwave cooling (Figure 1a) and longwave warming (Figure 1c) effects of the deep convective clouds over the tropical warm pool regions; the shortwave cooling moderately dominates, and the net TOA CRE effect (Figure 1e) is a weak cooling. Notable shortwave cooling is also prevalent over subtropical low

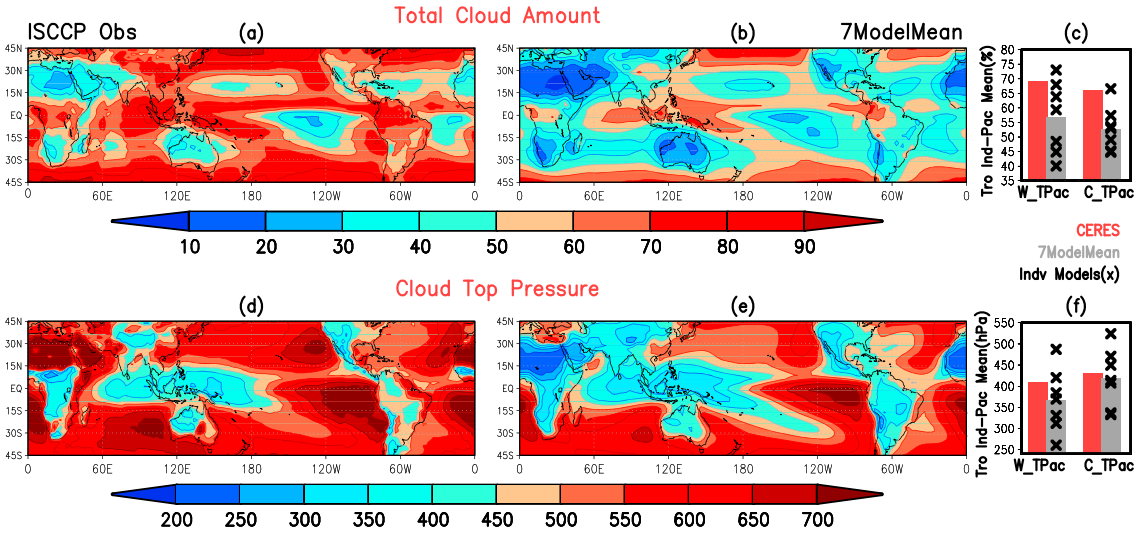

Figure 2. The annual mean climatology (1984–2007) of total cloud amount (%) in (a) the ISCCP observations, (b) the 7-model mean from the CMIP5 ISCCP satellite simulator output, and (c) the comparison between the ISCCP observations (red bar), the 7-model mean (gray bar), and the seven individual models (multiplication sign) in their regional means over the western tropical Pacific (100°E-140°E; 10°S-10°N) and central tropical Pacific (160°E-200°E; 10°S-10°N). Figures 2d–2f show the same as Figures 2a–2c except for cloud top pressure (hPa).

stratocumulus regions where it dominates the local strong net cooling effect. The multi-model mean agrees with the observations in large-scale features (not shown), with however notable regional differences. The multi-model mean considerably overestimates the TOA shortwave cooling (Figure 1b) and longwave warming (Figure 1d) over the western tropical Indian Ocean, central and eastern equatorial Pacific, subtropical Pacific, and western tropical Atlantic, and underestimates the TOA CREs near the Maritime Continent. The multi-model mean also strongly underestimates the shortwave cooling over the subtropical stratocumulus regions. The model bias in the shortwave CRE is larger than that in the longwave CRE; the net CRE (Figure 1f) shows a weak overestimation over the western tropical Indian Ocean, the equatorial Pacific, central subtropical Pacific, and subtropical Atlantic, and a distinct underestimation over the stratocumulus regions in the subtropical Pacific and Atlantic. The majority of the seven models agree with the multi-model mean in the sign of the TOA CRE biases while at varying magnitudes (not shown).

The CMIP5 model biases in Figure 1 are overall similar to those in *Wang and Su* [2013] and *Allan et al*. [2014] which are based on different combinations of CMIP5 models. Comparing the CMIP5 model mean biases in TOA CREs with those in clouds from the Cloud-Aerosol Lidar and Infrared Pathfinder Satellite Observation (CALIPSO) [*Chepfer et al*., 2010] satellite simulator output, *Wang and Su* [2013] show that the strong model overestimation (underestimation) of TOA CREs over tropical convective regions is mainly associated with the more (less) high clouds in the CMIP5 models, whereas the notable underestimation of shortwave cooling over the subsiding eastern subtropical oceans is associated with the lack of low stratocumulus clouds in the models. The model underestimation of TOA CREs and high clouds along the ITCZ regions and the overestimation over the Pacific trade cumulus regions reflect the double ITCZ biases in the CMIP5 models. Meanwhile, the model underestimation of high clouds and TOA CREs over the Maritime Continent and the overestimation over the western tropical Indian Ocean suggest that the CMIP5 models are still deficient in resolving the land-sea contrast and diurnal cycle over the Maritime Continent.

We next evaluate CMIP5 model simulations of climatologies of clouds. Figure 2 compares the CMIP5 model simulations with the ISCCP observations in their total cloud amount (Figures 2a–2c) and CTP (Figures 2d–2f) climatologies (1984–2007) in the tropics. The CMIP5 multi-model mean is generally consistent with the observations in large-scale spatial patterns, with however notable differences in magnitude. Consistent with the observations, the multi-model mean shows the maximum total cloud amount and minimum CTP over the tropical deep convective regions. Different from the observations, however, the CMIP5 multi-model mean shows notably smaller total cloud amount and higher cloud top over both the western and central tropical Pacific. The regional means of total cloud amount (areal percentage) over the western and

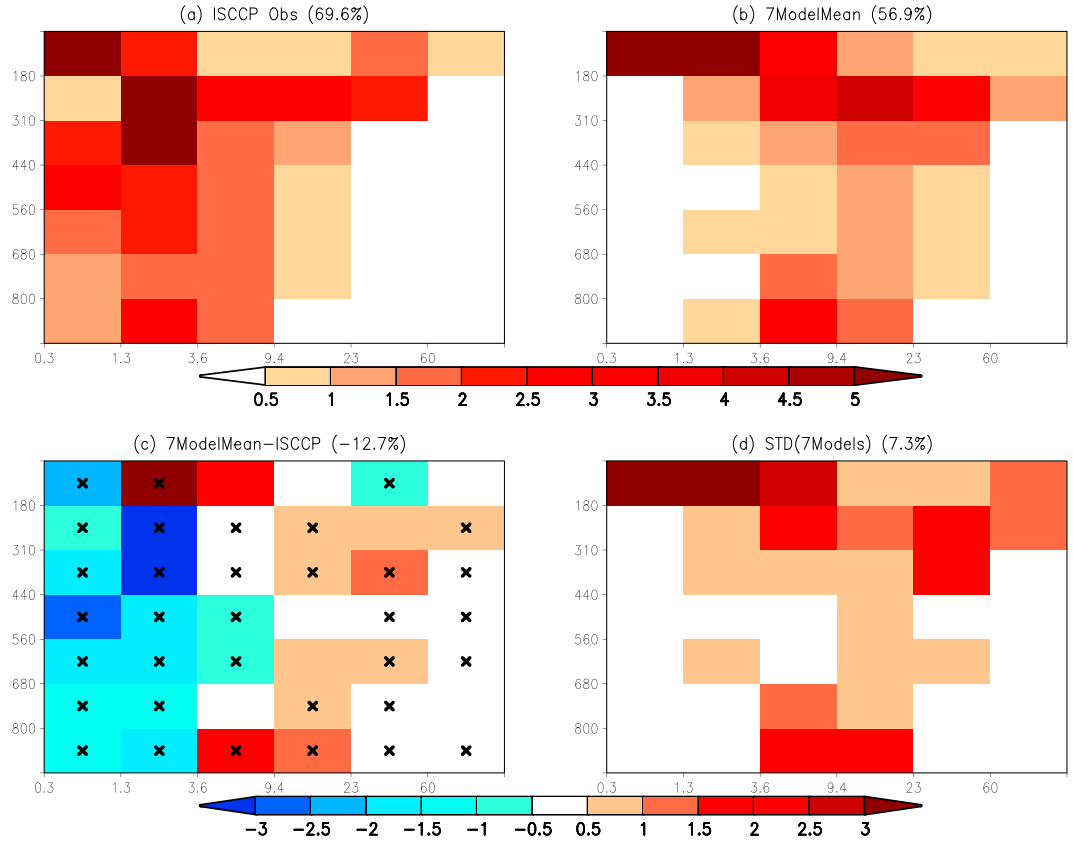

Figure 3. The annual mean climatology (1984–2007) of the joint histogram of cloud top pressure (CTP) and cloud optical thickness (τ) for cloud fraction (%) averaged over the tropical Indo-Pacific (60°E-200°E; 10°S-10°N), for (a) the ISCCP observations, (b) the 7-model mean from the CMIP5 ISCCP satellite simulator output, (c) the 7-model mean minus the ISCCP observations, in which CTP-τ bins with at least five of the seven CMIP5 models agree on the sign of the field plotted are marked with a multiplication sign, and (d) the standard deviation of the seven models relative to the 7-model mean. The sum of all CTP-τ bins for each panel is shown in its title.

central tropical Pacific in the multi-model mean are respectively 56.8% and 52.8%, considerably smaller than their observational counterparts which are respectively 69.3% and 66.2%. Furthermore, for both regions, six of seven CMIP5 models underestimate the regional mean total cloud amount. As for CTP, over the western tropical Pacific, the multi-model mean (366 hPa) has a cloud top 44 hPa higher than the observations (410 hPa), and five of seven CMIP5 models agree with the multi-model mean in showing a higher cloud top by underestimating CTP. By comparison, the multi-model mean cloud top (419 hPa) is only slightly higher than the observations (429 hPa) over the central tropical Pacific. Both the western and central tropical Pacific show substantial inter-model variations: the model CTP over the western tropical Pacific ranges from 487 hPa for MIROC5 to 261 hPa for GFDL-CM3 and that over the central tropical Pacific ranges from 524 hPa for MIROC5 to 333 hPa for CanAM4.

The distinct CTP differences between the multi-model mean and the observations over Sahara likely reflect the limitation of the ISCCP passive sensors in capturing local high thin clouds [*Klein et al.*, 2013]. They have little effect on tropical Indo-Pacific—the focus of our study, so are not a concern here.

We next focus on the tropical Indo-Pacific region (60°E-200°E; 10°S-10°N) where the atmospheric effects of ENSO dominate, and evaluate in Figure 3 and Table 2 the CMIP5 model simulations of climatological (1984–2007) joint CTP-τ histogram of cloud fraction. Figure 3a shows that the observed total cloud fraction (69.6%) is dominated by high clouds, while the high clouds are primarily contributed by thin clouds and secondarily by medium and thick clouds. Both the middle and low clouds are primarily thin and make secondary contributions to the total cloud fraction. The multi-model mean total cloud fraction (56.9%) (Figure 3b) is notably smaller than that of the observations (69.6%). The multi-model mean agrees with the

Table 2. The Comparison Between the Observations and the 7-Model Mean in ISCCP Cloud Fraction (%) Climatologies and Anomalies Associated With ENSO (Anomalies Shown in Parentheses) at a Reduced-Resolution Joint CTP-τ Histogram[a]

ISCCP Cloud Fraction Climatologies (Anomalies) (%)		Western Tropical Pacific		Central Tropical Pacific	
		Observations	7-Model Mean	Observations	7-Model Mean
High	Thin	27.5 (−3.5)	16.6 (−1.3)	25.5 (3.4)	14.7 (2.3)
	Medium	11.3 (−2.4)	15.1 (−1.8)	8.8 (2.1)	12.7 (3.2)
	Thick	5.5 (−1.0)	8.8 (−1.0)	5.0 (1.2)	6.5 (1.6)
Middle	Thin	7.9 (−0.2)	0.8 (0.1)	9.6 (0.9)	1.5 (−0.1)
	Medium	5.8 (−0.3)	3.7 (−0.1)	4.0 (0.3)	3.9 (0.3)
	Thick	0.7 (0.0)	2.4 (0.0)	0.4 (0.0)	1.7 (0.1)
Low	Thin	5.7 (1.2)	1.3 (0.1)	9.0 (−0.9)	1.9 (−0.4)
	Medium	4.7 (1.0)	6.8 (0.4)	3.8 (−0.5)	8.9 (−1.1)
	Thick	0.2 (0.0)	1.3 (0.1)	0.2 (0.0)	1.0 (−0.2)
Total		69.3 (−5.1)	56.8 (−3.5)	66.2 (6.4)	52.8 (5.7)

[a]See section 2 for definitions of high, middle, low clouds, and thin, medium, and thick clouds.

observations in the dominance of high clouds for the total cloud amount; it however shows distinct biases in τ regimes. The multi-model mean lacks thin clouds except for CTP $<$ 180 hPa and shows the prominence of medium and thick clouds. Compared with the observations in which thin, medium, and thick clouds respectively account for 60%, 31%, and 9% of the total cloud fraction, the thin, medium, and thick clouds in the multi-model mean represent 32%, 49%, and 19% of the total cloud fraction, respectively. The multi-model mean biases in simulating less total cloud amount yet higher cloud reflectivity are further highlighted in their difference distribution (Figure 3c), which shows the distinct multi-model mean underestimation of thin clouds and moderate overestimation of medium and thick clouds. The multiplication marks in Figure 3c indicate that the above multi-model mean biases in τ regimes are consistently present in most of the seven CMIP5 models.

We further examine the distribution of climatological joint CTP-τ histogram of cloud fraction in individual models (not shown). The results show that while all the seven models consistently produce clouds that are optically thicker than the observed, the CTP-τ bins that have the major contributions to the total cloud fraction vary greatly from model to model (not shown). The standard deviation of the cloud fraction in the seven CMIP5 models relative to their multi-model mean (Figure 3d) illustrates the substantial inter-model differences in the medium and thick cloud regimes, indicating the rather large model diversity in representing the tropical deep convective clouds.

We note that while not shown here, the results for the western tropical Pacific and central tropical Pacific are very similar to those for the tropical Indo-Pacific in Figure 3, except that the central tropical Pacific shows slightly weaker magnitudes.

3.2. Anomalies Associated With ENSO

To examine the relationships between ENSO and the year-to-year variations of TOA CREs, we compare the MEI with the time series of deseasonalized TOA CRE anomalies averaged over the western and central tropical Pacific (Figure 4). Over the western tropical Pacific, the time series of the shortwave CRE anomalies closely follows that of the MEI, with a temporal correlation of 0.61: the shortwave CRE shows positive anomalies for the warm phase of ENSO and negative anomalies for the cold phase of ENSO. The longwave CRE anomalies show the exact opposite distribution to the shortwave CRE anomalies, with somewhat weaker magnitude; its temporal correlation with MEI is −0.64. The opposite of the above occurs over the central tropical Pacific, with the magnitudes for shortwave CRE and longwave CRE anomalies respectively larger than those over the western tropical Pacific by 29% and 15%. The temporal correlations with the MEI are also higher over the central tropical Pacific: −0.69 for shortwave CRE and 0.74 for longwave CRE (Figure 4). The fairly good correspondence between the TOA CRE anomalies and the MEI suggests the dominant effect of ENSO on the TOA CRE changes over these regions. Thus, the TOA CRE anomalies associated with ENSO can be quantified by linearly regressing the TOA CRE anomalies against the MEI using least squares. Figure 4 also shows that such linear regression results by design correspond to the warm phase of ENSO. For convenience, the rest of the discussions on the anomalies associated with ENSO

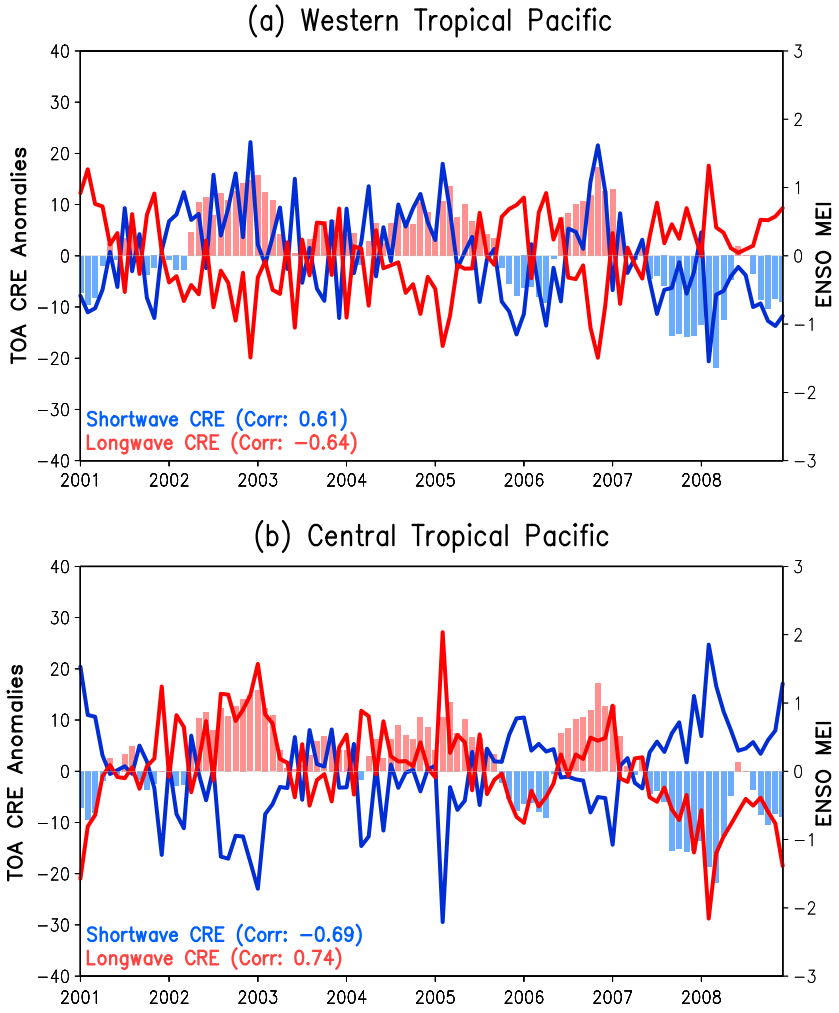

Figure 4. The time series of deseasonalized CERES EBAF shortwave (blue line) and longwave (red line) TOA CRE anomalies (W m^{-2}) averaged over (a) the western tropical Pacific (100°E-140°E; 10°S-10°N), and (b) the central tropical Pacific (160°E-200°E; 10°S-10°N) for January 2001-December 2008. The Multivariate ENSO Index (MEI) for the same period is shown in color bars. Also shown on each panel are the temporal correlations between the regional mean TOA CRE anomalies and the MEI.

will focus on the warm phase of ENSO, with the implications that the anomalies during the cold phase of ENSO show the same regional distribution but with an opposite sign.

Figure 5 compares the multi-model mean with the CERES EBAF in the regional distribution of the TOA CRE anomalies associated with ENSO, obtained using the abovementioned linear regression analysis against the MEI. Figures 5a and 5d show that during the warm phase of ENSO, the observed shortwave cooling and longwave warming are notably stronger in the central and eastern tropical Pacific, yet considerably weaker over the western tropical Pacific. These anomalies are associated with the enhanced (weakened) tropical convection and more (less) high clouds over the central (western) tropical Pacific that occur during a typical El Niño. Consistent with previous studies [e.g., *Cess et al.*, 2001b], there are strong cancelations between the shortwave and longwave TOA CRE anomalies over both the western and central tropical Pacific, and the net TOA CRE anomaly is a weak net warming over the Maritime Continent and a weak cooling along central equatorial Pacific (Figure 5g).

The TOA CRE anomalies in the CMIP5 multi-model mean (Figures 5b and 5e) agree with those in the CERES EBAF fairly well in spatial pattern, with a pattern correlation of 0.78 for shortwave CRE and 0.86 for longwave CRE. Among the seven models, the spatial pattern correlations for shortwave TOA CRE anomalies range from 0.52 for CNRM-CM5 to 0.69 for HadGEM2-A, whereas those for the longwave TOA

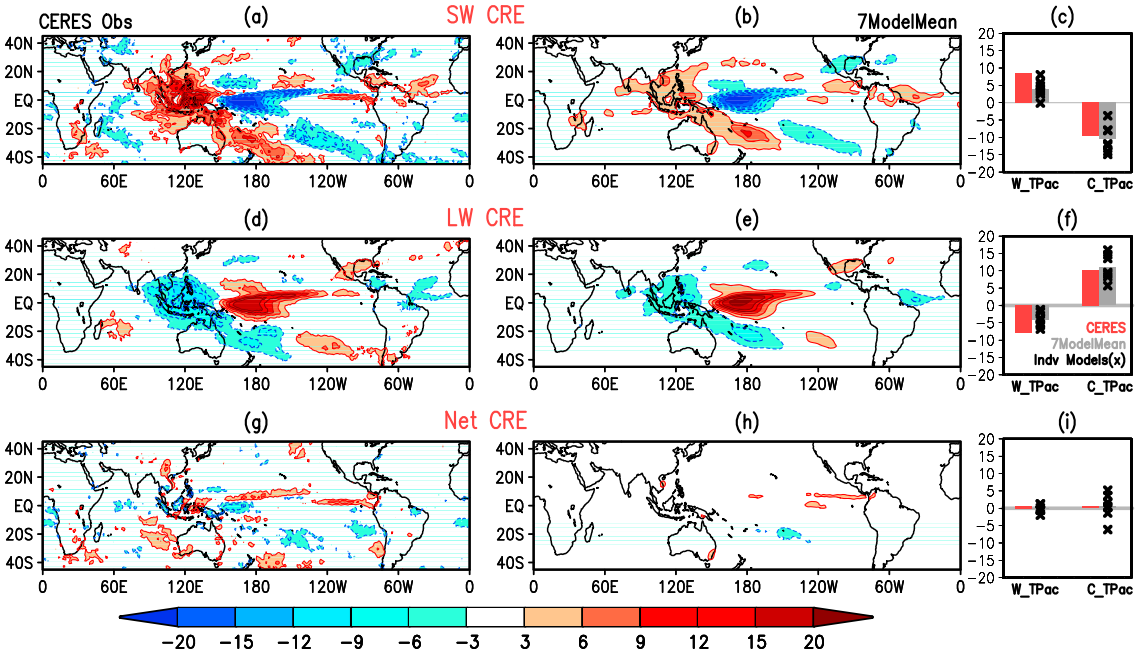

Figure 5. The tropical shortwave TOA CRE anomalies (W m^{-2}) associated with ENSO in (a) the CERES EBAF Edition 2.7 observations, (b) the 7-model mean, and (c) the comparison between the CERES observations (red bar), the 7-model mean (gray bar), and the seven individual models (multiplication sign) in their regional means over the western tropical Pacific (100°E-140°E; 10°S-10°N) and central tropical Pacific (160°E-200°E; 10°S-10°N); Figures 5d–5f show the same as Figures 5a–5c except for longwave TOA CRE anomalies associated with ENSO; Figures 5g–5i show the same as Figures 5a–5c except for the net TOA CRE anomalies associated with ENSO.

CRE anomalies range from 0.57 for CNRM-CM5 to 0.82 for CanAM4. In terms of magnitudes of the shortwave and longwave TOA CRE anomalies, the multi-model mean is comparable to the CERES observations over the central tropical Pacific but underestimates the observations by about 50% over the western tropical Pacific. An examination of the model spread in Figures 5c, 5f, and 5i shows the rather large inter-model variations over the central tropical Pacific, where the good multi-model mean simulation is essentially a result of strong cancelations among the seven models. By comparison, all the seven models consistently underestimate the observed TOA shortwave and longwave CRE anomalies over the western tropical Pacific, though at varying magnitudes. The CMIP5 model underestimation of TOA shortwave and longwave CRE anomalies over the western tropical Pacific could be related to the model underestimation of TOA shortwave and longwave CRE climatologies there (Figure 1).

We next evaluate model simulations of cloud anomalies associated with ENSO. Figure 6 compares the CMIP5 models with the ISCCP observations of total cloud amount and CTP anomalies during ENSO in the tropics. The agreement between the CMIP5 multi-model mean and the observations in spatial pattern is remarkable, with a pattern correlation of 0.84 for total cloud amount and a pattern correlation of 0.89 for CTP. The main model biases lie in the magnitudes of the anomalies. Over the western tropical Pacific, the multi-model mean notably underestimates the magnitude of cloud property changes; the total cloud amount reduction and cloud top drop in the multi-model mean are respectively 3.5% and 20 hPa, notably smaller than 5.1% and 36 hPa in the observations. In the central tropical Pacific, while the multi-model mean (5.7%) modestly underestimates the observations (6.4%) in total cloud amount increases, its CTP decrease (45 hPa) is notably larger than that of the observations (31 hPa). Figures 6c and 6f show that most of the seven models consistently underestimate the magnitude of cloud anomalies over the western tropical Pacific, whereas they exhibit rather large spread over the central tropical Pacific.

Figure 7 and Table 2 evaluate the CMIP5 model simulations in the joint CTP-τ histogram of cloud fraction anomalies during warm ENSO, averaged over the western tropical Pacific and the central tropical Pacific. The comparison between Figure 7 and Figure 3 shows the strong linkage between cloud climatology and cloud anomalies during ENSO for both observations and the CMIP5 models. The cloud changes during ENSO primarily occur in CTP-τ bins that have major contributions to the total cloud fraction climatologically. Over the western tropical Pacific, the observations (Figure 7a) show prominent reductions

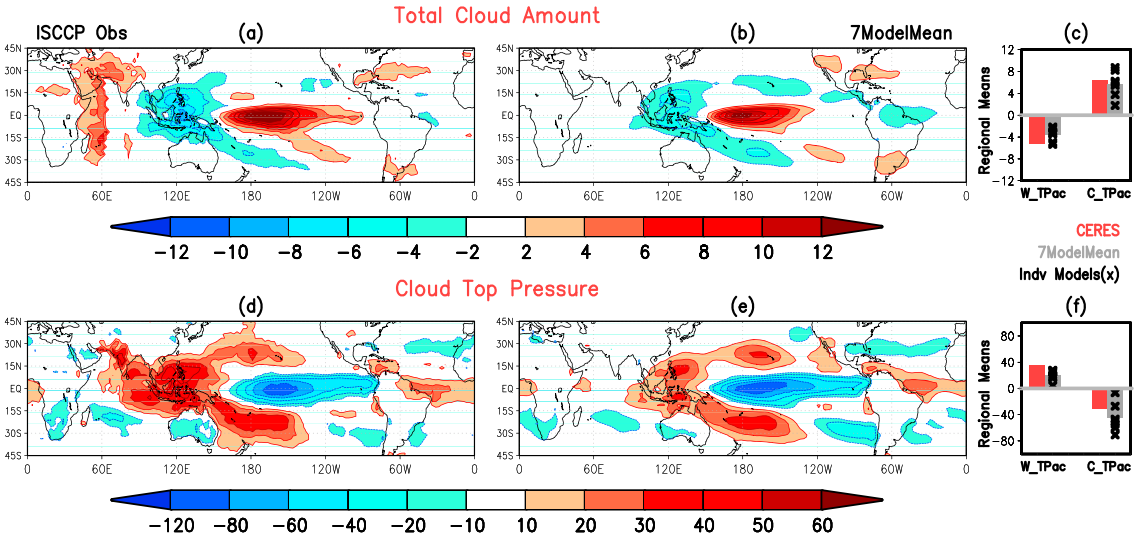

Figure 6. Same as Figure 2 except for total cloud amount (%) and cloud top pressure (hPa) anomalies associated with ENSO.

in high clouds (CTP $<$ 440 hPa)—primarily in high thin clouds and secondarily in high medium clouds, and modest increases in low thin and medium clouds (CTP $>$ 800 hPa; $1.3 < \tau < 9.4$). The multi-model mean (Figure 7b) agrees with the observations in the dominant reductions in high clouds. Associated with its climatological biases (Figure 3), however, the high cloud reductions in the multi-model mean mainly occur in the medium and thick cloud regimes; there are little changes in middle and low clouds. Furthermore, the multi-model mean underestimates the cloud changes in nearly all CTP-τ regimes. Table 2 shows that the reductions in high thin clouds and high medium and thick clouds in the multi-model mean are respectively −1.2% and −2.8%, considerably smaller than −3.5% and −3.4% in the observations. Meanwhile, the low cloud increase in the multi-model mean is only 0.6%, distinctly smaller than the observed 2.2%. The differences between the multi-model mean and the observations (Figure 7c) further highlight the strong model underestimation of high thin cloud decrease and low cloud increase. Such multi-model mean biases are commonly present in most of the seven CMIP5 models, though there is notable model diversity in high medium and thick cloud regimes (Figure 7d).

The cloud changes over the central tropical Pacific (Figures 7e–7g) are overall similar to those over the western tropical Pacific (Figures 7a–7c), except with an opposite sign and a notably larger magnitude. The observations (Figure 7e) show notable high cloud increases in all τ regimes, middle cloud increases in thin and medium cloud regimes, and a modest decrease in near-surface thin clouds. Note that while the low cloud decreases are likely real, there is potentially some contribution from the masking from higher cloud increases. The multi-model mean (Figure 7f) agrees with the observations in showing notable increases in high clouds and weak decreases in low clouds. These cloud changes, however, mainly occur in medium and thick cloud regimes. In contrast with the observations in which the increases in high thin clouds and high medium and thick clouds are respectively 3.4% and 3.3%, the multi-model mean shows the corresponding increases of 2.3% and 4.8% (Table 2). Figure 7g further highlights the multi-model mean biases in the τ domain by strongly underestimating the thin high cloud increases and moderately overestimating the increases in the medium and thick high clouds. Additionally, the multi-model mean produces a rather large increase in the very high cirrus clouds (CTP $<$ 90 hPa) and shows little change in middle clouds. Figure 7h shows the rather large inter-model differences in the medium and thick cloud regimes. The CTP-τ bins that have the major contributions to the total cloud fraction anomalies vary notably from model to model (not shown). An examination of individual models shows that the amount of high cloud changes during ENSO in a model is in general proportional to its climatological high cloud amount. The more climatological high clouds a model produces, the larger high cloud anomalies ENSO exerts in that model (not shown).

3.3. Quantifying TOA Radiative Effects of Tropical Clouds Using Cloud Radiative Kernels

In this subsection, we quantify the effects of cloud changes in various CTP-τ regimes on TOA CREs anomalies in both the observations and the CMIP5 models, using their respective cloud radiative kernels. The

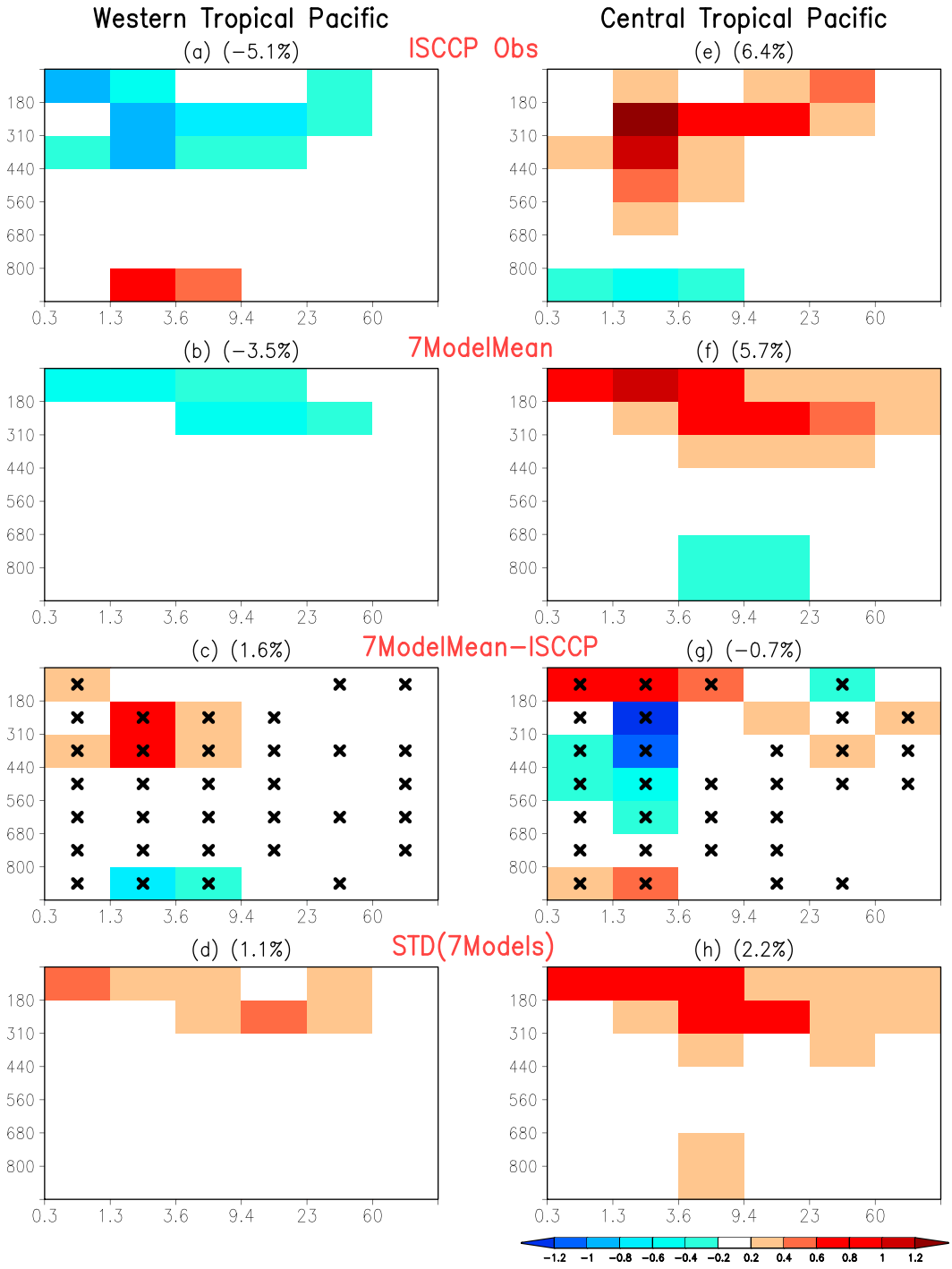

Figure 7. Same as Figure 3 except for the cloud fraction anomalies (%) associated with ENSO averaged over (a–d) the western tropical Pacific (100°E-140°E; 10°S-10°N) and (e–h) the central tropical Pacific (160°E-200°E; 10°S-10°N).

comparison between the observations and the CMIP5 models then shows the relative roles of model cloud biases in various CTP-τ regimes in contributing to the model biases in TOA CRE anomalies.

Figure 8 shows the joint CTP-τ histograms for the shortwave, longwave, and net cloud radiative kernels averaged over the tropical Indo-Pacific and 12 calendar months for the observations. The CTP-τ distributions of the cloud radiative kernels in Figures 8a, 8c, and 8e are largely consistent with those of the global annual mean cloud radiative kernels in *Zelinka et al.* [2012a, Figure 1], despite that they use a

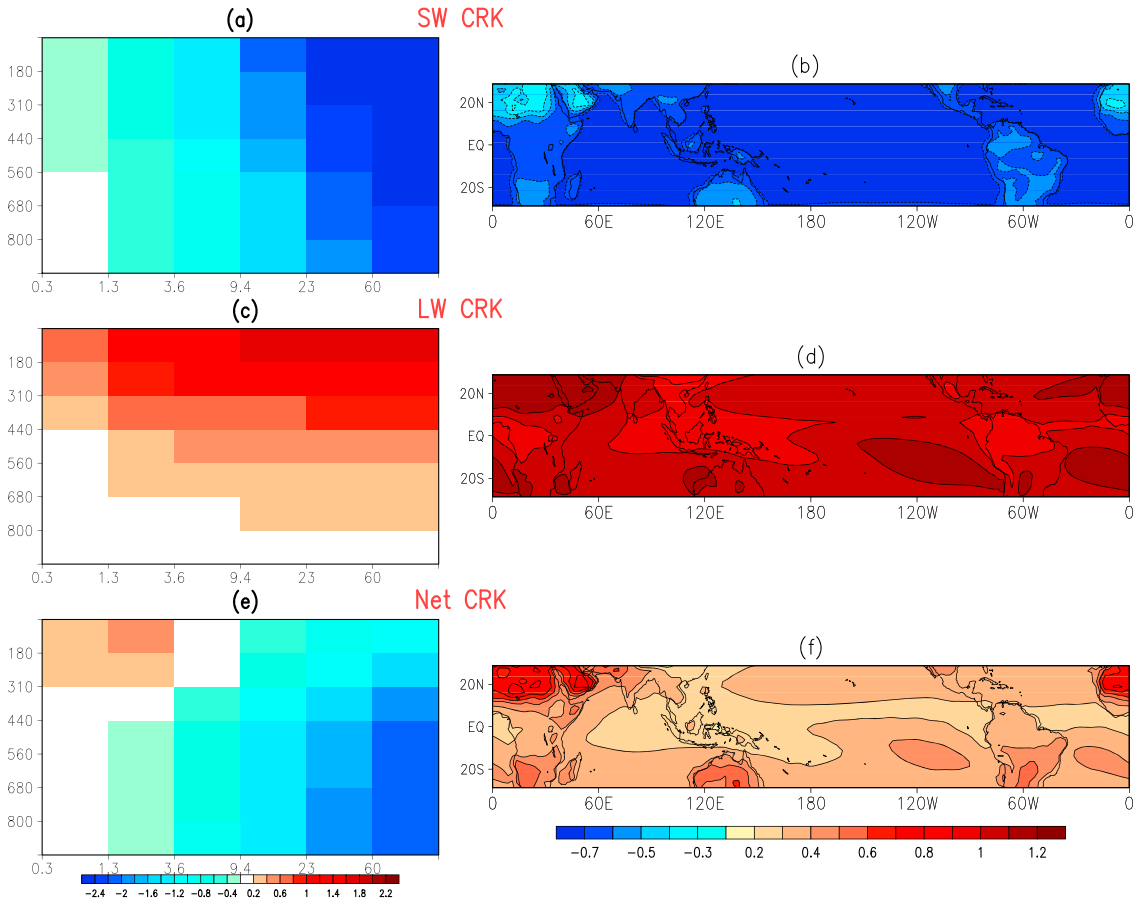

Figure 8. The shortwave cloud radiative kernel (W m^{-2} %$^{-1}$) (a) averaged over the tropical Indo-Pacific (60°E-200°E; 10°S-10°N) and 12 calendar months for the observations, and (b) latitude-longitude distribution for the CTP-τ bin (180 hPa < CTP < 310 hPa, 1.3 < τ < 3.6) that makes the largest contribution to the total cloud fraction for the ISCCP observations; (c and d) same as Figures 8a and 8b except for longwave cloud radiative kernel; (e–f) same as Figures 8a and 8b except for net cloud radiative kernel.

different set of model runs along with different assumptions including the simplifications of using zonal means. Such strong consistency suggests that the dependence of these kernels on CTP and τ is fairly a robust feature of the climate system. Consistent with *Zelinka et al.* [2012a], the tropical shortwave cloud radiative kernel mainly depends on τ and notably increases as clouds get thicker, while for thick clouds, the shortwave cloud radiative kernel also increases as cloud top gets higher. By comparison, the longwave cloud radiative kernel is largely a function of CTP and increases considerably as cloud top gets higher, and for thin clouds, it also increases as clouds get thicker. The longwave cloud radiative kernel overwhelms the shortwave cloud radiative kernel for high thin clouds, whereas the shortwave cloud radiative kernel dominates for the remaining CTP-τ bins, especially for low thick clouds. As a result, the net cloud radiative kernel shows a warming effect for high thin clouds and a cooling effect elsewhere.

Since the cloud radiative kernels are derived for each tropical longitude-latitude grid and incorporate the effects of the prescribed zonally varying temperature and specific humidity, they exhibit notable regional variations. Figures 8b, 8d, and 8f show the regional distributions of the cloud radiative kernels for the CTP-τ bin (180 hPa < CTP < 310 hPa and 1.3 < τ < 3.6), a bin that contributes substantially to the observed total cloud fraction over the tropical Indo-Pacific (Figure 3). When a spatially and optically uniform high thin cloud (180 hPa < CTP < 310 hPa, 1.3 < τ < 3.6) perturbation of 1% is applied, the tropical TOA shortwave CRE (Figure 8b) shows distinct land-sea contrast and is stronger over ocean than over land. It is largely zonally invariant over the tropical ocean with a value of −0.7 W m^{-2} %$^{-1}$, yet shows strong regional dependence over tropical land; regions with larger surface albedo tend to have weaker TOA shortwave CRE changes, and vice versa. The longwave cloud radiative kernel (Figure 8d) shows a notable

zonal asymmetry over both tropical ocean and land. It is relatively weak over the moisture-abundant tropical deep convective regions (0.9 W m^{-2} %$^{-1}$) and relatively strong over the dry subtropical subsidence regions (1.2 W m^{-2} %$^{-1}$). This suggests that the same amount of cloud fraction perturbation can lead to larger TOA longwave CRE changes over the subsidence regions than over the ascent regions. Such regional distribution reflects the spatial variability in the opacity of the clear-sky atmosphere, which is primarily driven by atmospheric moisture. For the high thin cloud (180 hPa $<$ CTP $<$ 310 hPa, $1.3 < \tau < 3.6$), the longwave kernel dominates the shortwave kernel, particularly over the tropical and subtropical subsidence regions; the net cloud radiative kernel (Figure 8f) shows a moderate warming: ~0.2 W m^{-2} %$^{-1}$ over the Indo-Pacific deep convective regions and ~0.4 W m^{-2} %$^{-1}$ over the subtropical subsidence regions. While not shown here, the spatial patterns of the shortwave and longwave cloud radiative kernels for other CTP-τ bins are largely similar to those in Figures 8b, 8d, and 8f, with the main differences in magnitude. For low clouds, the shortwave kernel displays some moderate zonal asymmetries over the tropical ocean, whereas the longwave kernel mainly shows a weak warming over subtropical subsidence regions. The distributions of the cloud radiative kernels based on the multi-model mean (not shown) are largely similar to those based on the observations in Figure 8. We note that the effects of CMIP5 model biases in cloud radiative kernels are negligible compared with those in model cloud fraction anomalies in accounting for the model biases in the TOA CRE anomalies due to ENSO (not shown).

Figure 8 suggests that the effects of model cloud biases in various CTP-τ regimes on TOA CREs must be scaled by their cloud radiative kernels. Thus, while the CMIP5 models strongly underestimate thin cloud changes (Figure 7), these cloud biases may not be manifested as strongly in the TOA CRE anomalies, because of the overall small TOA radiative effects of thin clouds. Likewise, while the CMIP5 models only moderately overestimate the medium and thick high clouds, their contribution to the biases in TOA radiative anomalies can be fairly large.

We next obtain the cloud-induced joint CTP-τ histogram of the TOA CRE anomalies due to ENSO by first multiplying the deseasonalized ISCCP joint CTP-τ histogram of cloud fraction anomalies (Figure 7) by the derived monthly cloud radiative kernels (Figure 8), element by element, and then linearly regressing such time series against the MEI. Such calculations are performed for both the observations and the CMIP5 models. Figure 9 and Table 3 show their comparison over the western tropical Pacific. The observations (Figure 9a) show that the strong reductions in high clouds (Figure 7a) lead to notably weakened shortwave cooling (8.2 W m^{-2} reduction) and weaker longwave warming (6.8 W m^{-2} reduction) CREs, whereas the moderate increase in low clouds contributes to a moderately strengthened shortwave cooling (1.5 W m^{-2} greater). The effects of high cloud changes dominate, and the net TOA CRE weakens. While the cloud reductions in medium and thick cloud regimes account for about ½ of total cloud reductions over the western tropical Pacific (Figure 7), they explain 76% of total shortwave TOA CRE anomalies and 60% of total longwave TOA CRE anomalies. Between the shortwave and longwave TOA CRE anomalies, the longwave TOA CRE anomalies dominate in high thin cloud regimes, and the shortwave TOA CRE anomalies dominate in the remaining cloud regimes.

The multi-model mean (Figure 9b) agrees with the observations (Figure 9a) in the dominant contribution of high cloud reductions for the weakened TOA CREs but distinctly differs from the observations in τ regimes as well as the contributions from middle and low clouds. Unlike those in the observations (Figure 9a), the weakened TOA CREs in the multi-model mean are predominantly due to the reductions in medium and thick clouds (Figures 9b and 9c), with little contributions from the middle and low clouds. The effects of model biases in cloud fraction anomalies on their TOA shortwave and longwave anomalies are scaled strongly by the cloud radiative kernels. For example, the multi-model mean underestimations of cloud reduction over the western tropical Pacific during ENSO (Figure 7c) are 2.2% (cloud fraction percentage) for high thin clouds and 0.5% for high medium and thick clouds. Since medium and thick clouds are notably more effective than thin clouds in exerting changes in TOA shortwave CREs (Figure 8), the above multi-model mean biases in high cloud reductions in thin clouds and medium and thick clouds respectively lead to biases of -1.3 and -0.8 W m^{-2} for TOA shortwave CRE anomalies (Table 3). Likewise, while the multi-model mean notably underestimates the low cloud increase and lacks middle cloud changes (Figure 7c), these low and middle cloud biases have negligible contribution to the model biases in TOA longwave CRE anomalies. For example, the low cloud increase during ENSO in the multi-model

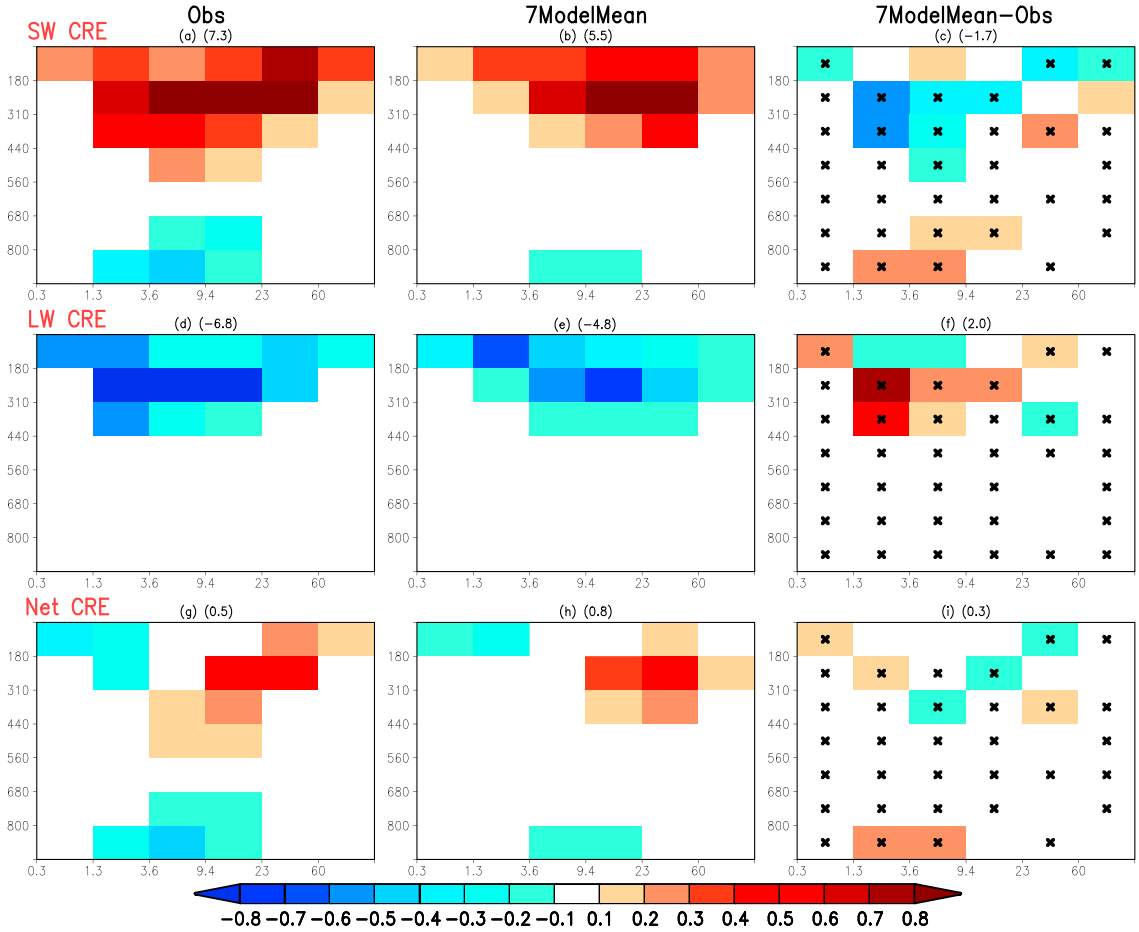

Figure 9. The kernel-derived joint CTP-τ histogram for TOA shortwave CRE anomalies (W m^{-2}) associated with ENSO averaged over the western tropical Pacific (100°E-140°E; 10°S-10°N) for (a) the ISCCP observations, (b) the 7-model mean from the CMIP5 ISCCP satellite simulator output, (c) the 7-model mean minus the ISCCP observations, in which CTP-τ bins with at least five of the seven CMIP5 models agree on the sign of the field plotted are marked with a multiplication sign; Figures 9d–9f show the same as Figures 9a–9c except for TOA longwave CRE anomalies; Figures 9g–9i show the same as Figures 9a–9c except for TOA net CRE anomalies. The sum of all CTP-τ bins for each panel is shown in its title.

Table 3. The Comparison Between the Observations and the 7-Model Mean in the Kernel-Derived Cloud-Induced TOA CRE Anomalies (W m^{-2}) Associated With ENSO at a Reduced-Resolution Joint CTP-τ Histogram[a]

Kernel-Derived TOA CRE Anomalies (W m^{-2})		Western Tropical Pacific				Central Tropical Pacific			
		Observations		7-Model Mean		Observations		7-Model Mean	
		SW	LW	SW	LW	SW	LW	SW	LW
High	Thin	2.0	−2.7	0.7	−1.2	−2.3	2.9	−1.3	2.2
	Medium	3.8	−2.7	3.0	−2.3	−3.5	2.7	−5.3	4.2
	Thick	2.4	−1.3	2.4	−1.3	−3.1	1.8	−4.2	2.1
Middle	Thin	0.1	−0.1	0.0	0.0	−0.4	0.3	0.0	0.0
	Medium	0.4	−0.1	0.1	0.0	−0.4	0.2	−0.4	0.1
	Thick	0.0	0.0	0.0	0.0	0.1	0.0	−0.2	0.1
Low	Thin	−0.4	0.1	0.0	0.0	0.3	0.0	0.2	0.0
	Medium	−1.0	0.1	−0.5	0.0	0.6	−0.1	1.3	−0.2
	Thick	−0.1	0.0	−0.2	0.0	0.1	0.0	0.3	0.0
Total		7.3	−6.8	5.5	−4.8	−8.7	7.7	−9.5	8.5

[a]See section 2 for definitions of high, middle, low clouds, and thin, medium, and thick clouds.

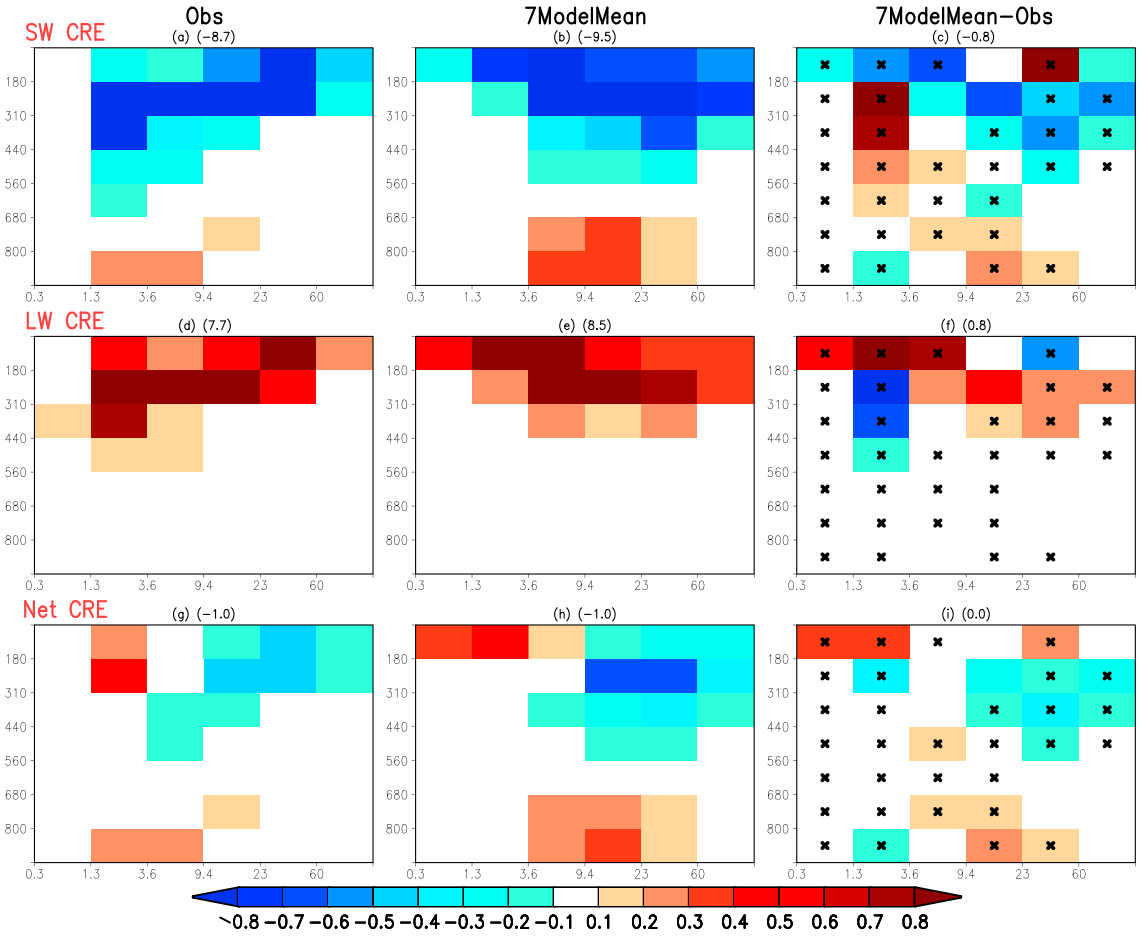

Figure 10. Same as Figure 9 except for the central tropical Pacific (160°E-200°E; 10°S-10°N).

mean is only 0.6%, notably smaller than 2.2% in the observations (Table 2); the corresponding multi-model mean bias in TOA longwave CRE anomalies, however, is only $-0.2\,\mathrm{W\,m^{-2}}$ (Table 3). When summed over all CTP-τ bins, the total cloud-induced shortwave and longwave TOA CRE anomalies in the multi-model mean are respectively 25% and 30% weaker than those of the observations, a result of an overall model underestimation of cloud changes over the western tropical Pacific (Figure 7c) combined with the scaling effects of the cloud radiative kernels (Figure 8).

Figure 10 shows the joint CTP-τ histogram for the cloud-induced TOA CRE anomalies averaged over the central tropical Pacific. During warm ENSO, the enhanced TOA shortwave cooling and longwave warming anomalies in the observations are primarily contributed by high cloud increases. The middle cloud increases make a moderate contribution to the enhanced shortwave cooling, while the decreases in low clouds from local anomalous ascent tend to weaken the shortwave cooling. The longwave warming anomalies dominate the shortwave cooling anomalies for high thin clouds, and the opposite occurs for the remaining CTP-τ bins. The comparison between the multi-model mean and the observations again reflects the effects of climatological model biases, particularly optically much thicker clouds and the lack of middle and low clouds. The TOA CRE anomalies in the multi-model mean are mainly due to the changes in medium and thick high clouds, with little contributions from thin clouds; there is little contribution from middle clouds. Despite the model cloud biases over the central tropical Pacific (cf. Figure 7g), through the modulating effects of the cloud radiative kernels, the TOA CRE biases from the moderate multi-model mean overestimation of medium and thick clouds are comparable to those from the strong underestimation of thin clouds. When summed over all the CTP-τ bins, the shortwave and longwave TOA CRE anomalies in the multi-model mean are about 10% stronger than those of the observations. Therefore,

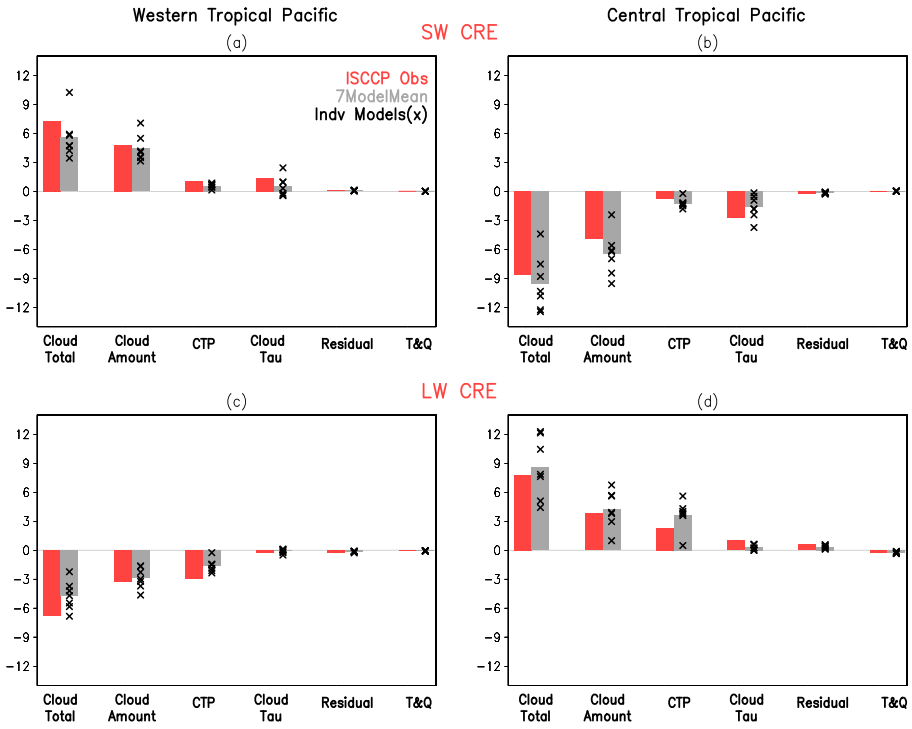

Figure 11. (a) The comparison between the observations (red bars), the 7-model mean (gray bars), and the seven individual models (multiplication sign) in terms of kernel-derived TOA CRE anomalies (W m^{-2}) summed over all CTP-τ bins averaged over the western tropical Pacific (100°E-140°E; 10°S-10°N), from the total cloud changes (first bar from left), total cloud amount changes only (second bar from left), changes in CTP only (third bar from left), changes in τ only (fourth bar from left), a residual component (fifth bar from left), and changes in temperature and humidity only (sixth bar from left); Figure 11b shows the same as Figure 11a except for the regional averages over the central tropical Pacific (160°E-200°E; 10°S-10°N); Figures 11c and 11d are the same as Figures 11a and 11b except for TOA longwave CRE anomalies.

the good multi-model mean simulation of TOA CRE anomalies over the central tropical Pacific does not necessarily indicate the good model performance over that region. Instead, it is a result of compensating errors between the multi-model mean underestimation of TOA CRE changes from thin clouds and the overestimation of TOA CRE changes from medium and thick clouds. The compensation arising from averaging across models with biases of either sign also likely plays a role.

In addition, while the net CRE anomaly biases in Figures 9 and 10 are small in most CTP-τ bins, they are however a result of substantial cancelations between the large biases in shortwave CRE anomalies and those in longwave CRE anomalies which have large magnitudes but of opposite sign.

3.4. Relative Roles of Changes in Cloud Properties, Temperature, and Humidity for TOA CRE Anomalies During ENSO

In this subsection, we assess the CMIP5 model representations of the relative roles of changes in cloud properties as well as temperature and humidity in contributing to the TOA CRE anomalies during ENSO. Figure 11 shows the cloud-induced TOA CRE anomalies, the contributions from the changes in individual cloud components (cloud amount, CTP, and τ), and a residual component, as well as the changes in temperature and humidity during ENSO, averaged over the western tropical Pacific and central tropical Pacific. The results for the observations show that over both the western and central tropical Pacific, the changes in total cloud amount, CTP, and τ all contribute to the cloud-induced shortwave and longwave CRE anomalies associated with ENSO (Figures 11a and 11b), whereas the residual component makes an overall negligible contribution. The shortwave cooling anomalies are primarily contributed by the total cloud amount changes and secondarily by the changes in CTP and τ. Specifically, the local changes in total cloud amount, CTP, and τ respectively contribute to 66%, 14%, and 18% of the weakened shortwave cooling (7.3 W m^{-2}) over the western tropical Pacific, and 57%, 9%, and 31% of the enhanced shortwave

cooling ($-8.7\,W\,m^{-2}$) over the central tropical Pacific. By comparison, over the western and central tropical Pacific, the changes in both total cloud amount and CTP contribute considerably to the cloud-induced TOA longwave CRE anomalies (Figures 11c and 11d), whereas the changes in τ play negligible roles. The local changes in total cloud amount, CTP, and τ respectively contribute to 49%, 44%, and 4% of the weakened longwave warming ($-6.8\,W\,m^{-2}$) over the western tropical Pacific, and 49%, 30%, and 13% of the enhanced longwave warming ($7.8\,W\,m^{-2}$) over the central tropical Pacific. The effects of temperature and humidity changes are overall negligible for both shortwave and longwave CRE anomalies.

The relative roles of the observed changes in cloud property and temperature and humidity for shortwave and longwave TOA CRE anomalies in Figure 11 are overall qualitatively consistent with those in *Sun et al*. [2012], even though their results were based on a single ENSO event and were obtained using different methodology with different observational data inputs.

The multi-model mean overall agrees with the observations. Consistent with those in the observations, the kernel-derived TOA shortwave CRE anomalies in the multi-model mean are primarily from the total cloud amount changes and secondarily from changes in CTP and τ. The local changes in total cloud amount, CTP, and τ in the multi-model mean respectively contribute to 79%, 10%, and 9% of the weakened shortwave cooling ($5.6\,W\,m^{-2}$) over the western tropical Pacific, and 68%, 13%, and 17% of the enhanced shortwave cooling ($-9.5\,W\,m^{-2}$) over the central tropical Pacific. The TOA longwave CRE anomalies are notably contributed by both the total cloud amount changes and the changes in CTP, with little contributions from the changes in τ. The local changes in total cloud amount, CTP, and τ in the multi-model mean respectively contribute to 61%, 33%, and 2% of the weakened longwave warming ($-4.7\,W\,m^{-2}$) over the western tropical Pacific, and 50%, 43%, and 4% of the enhanced longwave warming ($8.5\,W\,m^{-2}$) over the central tropical Pacific. Furthermore, the changes in temperature and humidity have negligible contributions to the TOA CRE anomalies in the multi-model mean.

We next compare the observations and the CMIP5 multi-model mean for each of the components in Figure 11, to examine their relative roles in contributing to the multi-model mean biases in TOA CRE anomalies. Over the western tropical Pacific, the multi-model mean underestimation of cloud-induced shortwave TOA CRE anomalies (Figure 11a) mainly comes from the model biases in τ changes and secondarily from model biases in CTP changes. By comparison, the multi-model mean underestimation in cloud-induced longwave TOA CRE anomalies (Figure 11c) is mainly due to the model biases in CTP changes. Over the central tropical Pacific, the weak multi-model mean overestimation of cloud-induced TOA shortwave CRE anomalies (Figure 11b) is mainly contributed by model biases in changes in total cloud amount and CTP, which are partially negated by the model biases in changes in τ. The weak multi-model mean overestimation of TOA longwave CRE anomalies is mainly contributed by the model biases in changes in total cloud amount and CTP (Figure 11d) partially negated by the model biases in τ.

It is worth noting that while the total cloud amount changes dominate TOA shortwave CRE anomalies and account for about half of the longwave CRE anomalies in both observations and the multi-model mean (Figure 11), their exerted TOA shortwave and longwave CRE anomalies are comparable between the multi-model mean and the observations over the western tropical Pacific, thus contributing little to the notable multi-model mean underestimation of TOA CRE anomalies there (Figures 11a and 11c). The TOA radiative effects of total cloud amount changes during ENSO are by definition determined by the ratio of total cloud amount change to total cloud amount climatology, climatological CTP-τ distribution of clouds, and cloud radiative kernels. The ratios for total cloud amount changes are comparable between the observations (7.4%) and the CMIP5 multi-model mean (6.2%) over the western tropical Pacific, because the CMIP5 models underestimate the total cloud amount in both climatology (Figure 3) and anomalies (Figure 7) there. Meanwhile, although the CMIP5 models show distinct climatological biases in τ regimes by strongly underestimating thin clouds and moderately overestimating medium and thick clouds (Figure 3), when scaled by the cloud radiative kernels, the underestimation of TOA CRE anomalies from thin clouds is offset by the overestimation of TOA CRE anomalies from medium and thick clouds. Over the western tropical Pacific, with an increase of 1% of their respective total cloud amount, both the multi-model mean and the observations show an enhanced TOA shortwave cooling of $0.8\,W\,m^{-2}$ and longwave warming of $0.5\,W\,m^{-2}$. As a result, the accumulated TOA CRE effects between the observations ($5.7\,W\,m^{-2}$ for shortwave and $4.0\,W\,m^{-2}$ for longwave) and the multi-model mean ($5.1\,W\,m^{-2}$ for shortwave and

3.3 W m^{-2} for longwave) are comparable. Thus, the good multi-model mean simulation of TOA CRE anomalies from total cloud amount changes is essentially a result of compensating errors between model clouds at different τ regimes.

4. Summary and Conclusions

This study evaluates and investigates the CMIP5 model simulations of ENSO effects on tropical clouds and TOA CREs. The satellite-based observations used to evaluate the CMIP5 models include the CERES EBAF TOA radiative fluxes and the ISCCP joint CTP-τ histogram of cloud fraction. The ISCCP satellite simulator output from the CMIP5 AMIP simulations is used to evaluate the model clouds.

To quantify the relative roles of model cloud biases in various CTP-τ regimes in contributing to the model biases in TOA CRE anomalies during ENSO, we derive shortwave and longwave cloud radiative kernels [*Zelinka et al*., 2012a]—a measure of TOA CRE sensitivity to cloud fraction perturbations, and construct joint CTP-τ histogram for TOA CRE anomalies for both the observations and the CMIP5 model simulations. To evaluate the CMIP5 model simulation of the relative roles of changes in cloud properties for the TOA CRE anomalies during ENSO, we use the methodology in *Zelinka et al*. [2012b, 2013] and decompose the cloud-induced TOA CRE anomalies due to ENSO into those due to changes in total cloud amount, CTP, τ, and a residual component. Lastly, to assess the model representation of the effect of changes in temperature and humidity on TOA CRE anomalies, we repeat the above calculations but using temperature and humidity that are the sum of their climatologies and anomalies due to ENSO when deriving cloud radiative kernels, and then compare these two sets of calculations in their TOA CRE anomalies.

The results show that climatologically, most of the CMIP5 models underestimate the TOA CREs near the Maritime Continent, yet notably overestimate the TOA CREs over the central tropical Pacific. The CMIP5 models exhibit distinct biases in clouds over the tropical Indo-Pacific. They produce considerably less total cloud amount with notably higher cloud top than the observed. Further, all the CMIP5 models show distinct biases in τ regimes by simulating clouds that are optically much thicker than the observed. In contrast with the observations in which the total cloud fraction is primarily contributed by thin clouds, the CMIP5 models lack thin clouds and are dominated by medium and thick clouds. The models also lack middle clouds, and most of them strongly underestimate low clouds.

During ENSO, the CMIP5 models agree with the observations fairly well in the spatial pattern of shortwave and longwave TOA CRE anomalies, with however notable differences in magnitudes. In particular, the CMIP5 models consistently underestimate the shortwave and longwave TOA CRE anomalies over the western tropical Pacific, with their multi-model mean being only 50% of the observed. Over the central tropical Pacific, while the multi-model mean is comparable to the observations for both the shortwave and longwave TOA CRE anomalies, it is a result of strong cancelations between the CMIP5 models.

The model biases in cloud anomalies associated with ENSO are strongly affected by their biases in cloud climatology. During ENSO, the total cloud amount changes over the tropical Indo-Pacific in the CMIP5 models are notably smaller than those of the observed, particularly over the western tropical Pacific. Associated with the model climatological biases in simulating clouds that are optically much thicker than the observed, the majority of model cloud changes occur in the medium and thick cloud regimes. The CMIP5 models also strongly underestimate the changes in middle and low clouds. Additionally, the CMIP5 models considerably underestimate the cloud top pressure increases over the western tropical Pacific and notably overestimate the cloud top pressure decreases over the central tropical Pacific.

These distinct model biases in clouds are, however, not manifested strongly in TOA CREs, due to the strong error compensations in cloud optical thickness and cloud vertical structure, combined with the scaling effects of cloud radiative kernels. While the CMIP5 models strongly underestimate thin clouds and moderately overestimate medium and thick clouds, because of the notable dependence of shortwave cloud radiative kernels on τ, the model underestimation of TOA shortwave CRE anomalies from thin clouds is only moderately larger than the model overestimations of TOA shortwave CRE anomalies from medium and thick clouds. In addition, the low cloud changes are often of opposite sign of the high cloud changes, though with weaker magnitudes. The above compensations result in overall small TOA shortwave CRE biases when summed over all the CTP-τ bins. As for longwave CRE anomalies, because of the distinct

dependence of longwave cloud radiative kernels on CTP, the model biases in low and middle clouds have negligible effects on TOA longwave CRE anomalies. Further, the compensation between model underestimation of thin cloud changes and overestimation of medium and thick cloud changes contribute to the TOA longwave CRE anomalies as well, because of the moderate dependence of longwave cloud radiative kernel on τ for high clouds.

As for the relative roles of changes in cloud properties in contributing to the TOA CRE anomalies during ENSO, the CMIP5 multi-model mean agrees with the observations on the dominance of total cloud amount changes for shortwave TOA CRE anomalies and the considerable contributions from both total cloud amount changes and cloud top pressure (CTP) changes for longwave TOA CRE anomalies. The CMIP5 models are also consistent with the observations in the negligible effects of temperature and humidity changes on TOA shortwave and longwave CRE anomalies.

The comparison between the multi-model mean and the observations in contributions from individual cloud properties shows that the notable multi-model mean underestimation of cloud-induced TOA CRE anomalies over the western tropical Pacific is mainly due to the multi-model mean biases in CTP and τ changes for shortwave and CTP changes for longwave. By comparison, the TOA CRE anomalies from the total cloud amount changes are comparable between the observations and the multi-model mean, thus making little contribution to the notable multi-model mean underestimation of TOA CRE anomalies over the western tropical Pacific. This is essentially a result of compensating errors between multi-model mean underestimation of TOA CRE anomalies from thin clouds and its overestimation of TOA CRE anomalies from medium and thick clouds. The compensation from averaging across models with biases of either sign plays a secondary role. Over the central tropical Pacific, the weak multi-model mean overestimation of TOA CRE anomalies is mainly contributed by model biases in cloud amount and τ anomalies for shortwave and by model biases in changes in cloud amount and CTP for longwave.

This study shows that while the CMIP5 models simulate the tropical TOA CRE anomalies associated with ENSO well, they are rather deficient in simulating tropical cloud changes. The good model simulations of the TOA CRE anomalies are essentially a result of compensating model errors between different cloud processes. The model biases in cloud anomalies during ENSO are strongly affected by the model biases in cloud climatology, notably the considerable underestimation of total cloud amount with higher optical reflectivity, and the lack of middle and low clouds. These CMIP5 model errors in clouds primarily originate from the errors in the model cloud parameterizations [e.g., *Su et al*., 2012]. In addition, the common model biases in underestimating the TOA CRE and cloud changes over the western tropical Pacific are worth noting. In a fully coupled ocean-atmosphere model system, such model cloud biases over the western tropical Pacific can easily lead to biases in tropical SST whose effects can subsequently propagate into regions worldwide through atmospheric teleconnection. As a result, the produced coupled model simulations and projections of future climate change are subject to the above model cloud biases over the western tropical Pacific. Such model biases originate from the deficiencies in model convective parameterization schemes rather than model resolution [e.g., *Pearson et al*., 2014]. While some progress has been made by tuning model parameterization schemes, such as altering the dependence of entrainment on the surrounding atmospheric conditions [e.g., *Del Genio and Wu*, 2010], much modeling work is needed to correct this model bias. Overall, this study stresses the critical need to improve model simulation of clouds, not only in regional distribution (e.g., underestimations near Maritime Continent and double ITCZ bias) but also in cloud properties (e.g., smaller cloud amount with higher optical reflectivity). Only when these issues are alleviated can there be a stronger confidence in the model simulations of climate variability and projection of future climate change.

Acknowledgments

This study is supported by the NASA CLOUDSAT and CALIPSO Science Team Recompete program (NNH09ZDA001N-CCST). We acknowledge the World Climate Research Programme's Working Group on Coupled Modeling, which is responsible for CMIP, and we thank the climate modeling groups (listed in Table 1 of this paper) for producing and making available their model output. For CMIP, the U.S. Department of Energy's Program for Climate Model Diagnosis and Intercomparison provides coordinating support and led development of software infrastructure in partnership with the Global Organization for Earth System Science Portals. The CERES EBAF Edition 2.7 data were obtained from the NASA Langley Research Center CERES ordering tool at http://ceres.larc.nasa.gov/cmip5_data.php/. The ISCCP data were obtained from the website http://climserv.ipsl.polytechnique.fr/cfmip-obs/. We thank Mark Zelinka and two anonymous reviewers for their constructive comments and suggestions which have significantly improved this paper.

References

Allan, R. P., A. Slingo, and M. A. Ringer (2002), Influence of dynamics on the changes in tropical cloud radiative forcing during the 1998 El Niño, *J. Clim.*, *15*, 1979–1986.

Allan, R. P., C. Liu, N. G. Loeb, M. D. Palmer, M. Roberts, D. Smith, and P.-L. Vidale (2014), Changes in global net radiative imbalance 1985–2012, *Geophys. Res. Lett.*, *41*, 5588–5597, doi:10.1002/2014GL060962.

Cess, R. D., M. H. Zhang, P. H. Wang, and B. W. Wielicki (2001a), Cloud structure anomalies over the tropical Pacific during the 1997/98 El Niño, *Geophys. Res. Lett.*, *28*, 4547–4550, doi:10.1029/2001GL013750.

Cess, R. D., M. Zhang, B. A. Wielicki, D. F. Young, X.-L. Zhou, and Y. Nikitenko (2001b), The influence of the 1998 El Niño upon cloud-radiative forcing over the Pacific warm pool, *J. Clim.*, *14*, 2129–2137.

Chepfer, H., S. Bony, D. M. Winker, G. Cesana, J. L. Dufresne, P. Minnis, C. J. Stubenrauch, and S. Zeng (2010), The GCM oriented CALIPSO cloud product (CALIPSO-GOCCP), *J. Geophys. Res.*, *105*, D00H16, doi:10.1029/2009JD012251.
Del Genio, A. D., and J. Wu (2010), The role of entrainment in the diurnal cycle of continental convection, *J. Clim.*, *23*, 2722–2738.
Delworth, T. L., et al. (2012), Simulated climate and climate change in the GFDL CM2.5 high-resolution coupled climate model, *J. Clim.*, *25*, 2755–2781.
Dirmeyer, P. A., et al. (2012), Simulating the diurnal cycle of rainfall in global climate models: Resolution versus parameterization, *Clim. Dyn.*, *39*, 399–418.
Fu, Q., and K. N. Liou (1992), On the correlated k-distribution method for radiative transfer in nonhomogeneous atmospheres, *J. Atmos. Sci.*, *49*, 2139–2156.
Guilyardi, E., A. Wittenberg, A. Fedorov, M. Collins, C. Wang, A. Capotondi, G. J. van Oldenborgh, and T. Stockdale (2009), Understanding El Niño in ocean-atmosphere general circulation models: Progress and challenges, *Bull. Am. Meteorol. Soc.*, *90*, 325–340.
Hwang, Y.-T., and D. M. W. Frierson (2013), Link between the double-intertropical convergence zone problem and cloud biases over the Southern Ocean, *Proc. Natl. Acad. Sci. U.S.A.*, *110*(13), 4935–4940.
Jha, B., and A. Kumar (2009), A comparison of the atmospheric response to ENSO in coupled and uncoupled model simulations, *Mon. Weather Rev.*, *137*, 479–487.
Jin, Z., T. P. Charlock, W. L. Smith Jr., and K. Rutledge (2004), A parameterization ocean surface albedo, *Geophys. Res. Lett.*, *31*, L22301, doi:10.1029/2004GL021180.
Kato, S., N. G. Loeb, F. G. Rose, D. R. Doelling, D. A. Rutan, T. E. Caldwell, Y. Lisan, and R. A. Weller (2013), Surface irradiances consistent with CERES-derived top-of-atmosphere shortwave and longwave irradiances, *J. Clim.*, *26*, 2719–2740.
Klein, S. A., and C. Jakob (1999), Validation and sensitivities of frontal clouds simulated by the ECMWF model, *Mon. Weather Rev.*, *127*, 2514–2531.
Klein, S. A., Y. Zhang, M. D. Zelinka, R. N. Pincus, J. Boyle, and P. J. Gleckler (2013), Are climate model simulations of clouds improving? An evaluation using the ISCCP simulator, *J. Geophys. Res. Atmos.*, *118*, 1329–1342, doi:10.1002/jgrd.50141.
Latif, M., et al. (2001), ENSIP: The El Niño simulation intercomparison project, *Clim. Dyn.*, *18*, 255–276.
Li, G., and S.-P. Xie (2014), Tropical biases in CMIP5 multimodel ensemble: The excessive equatorial pacific cold tongue and double ITCZ problems, *J. Clim.*, *27*, 1765–1780.
Lin, J. L. (2007), The double-ITCZ problem in IPCC AR4 coupled GCMs: Ocean-atmosphere feedback analysis, *J. Clim.*, *20*, 4497–4525.
Liu, C., R. P. Allan, and G. J. Huffman (2012), Co-variation of temperature and precipitation in CMIP5 models and satellite observations, *Geophys. Res. Lett.*, *39*, L13803, doi:10.1029/2012GL052093.
Lloyd, J., E. Guilyardi, and H. Weller (2011), The role of atmosphere feedbacks during ENSO in the CMIP3 models. Part II: Using AMIP runs to understand the heat flux feedback mechanisms, *Clim. Dyn.*, *37*, 1271–1292.
Loeb, N. G., B. A. Wielicki, D. R. Doelling, G. L. Smith, D. F. Keyes, S. Kato, N. Manlo-Smith, and T. Wong (2009), Toward optimal closure of the Earth's TOA radiation budget, *J. Clim.*, *22*, 748–766.
Lu, R., B. Dong, R. D. Cess, and G. L. Potter (2004), The 1997/98 El Niño: A test for climate models, *Geophys. Res. Lett.*, *31*, L12216, doi:10.1029/2004GL019956.
Mace, G. G., S. Houser, S. Benson, S. A. Klein, and Q. Min (2011), Critical evaluation of the ISCCP simulator using ground-based remote sensing data, *J. Clim.*, *24*, 1598–1612.
Martin, G. M., et al. (2011), The HadGEM2 family of Met Office unified model climate configurations, *Geosci. Model Dev. Discuss.*, *4*, 765–841.
Mechoso, C. R., et al. (1995), The seasonal cycle over the tropical Pacific in coupled ocean-atmosphere general circulation models, *Mon. Weather Rev.*, *123*, 2825–2838.
Meehl, G. A., C. Covey, B. McAvaney, M. Latif, and R. J. Stouffer (2005), Overview of the coupled model intercomparison project, *Bull. Am. Meteorol. Soc.*, *86*, 89–93.
Mizuta, R., et al. (2012), Climate simulations using MRI-AGCM3.2 with 20-km grid, *J. Meteorol. Soc. Jpn.*, *90A*, 233–258.
Nagio, H., and Y. N. Takayabu (2013), Reproducibility of precipitation distribution over the tropical oceans in CMIP5 multi-climate models compared to CMIP3, *Clim. Dyn.*, *41*, 2909–2920.
Nam, C., S. Bony, J.-L. Dufresne, and H. Chepfer (2012), The 'too few, too bright' tropical low-cloud problem in CMIP5 models, *Geophys. Res. Lett.*, *39*, L21801, doi:10.1029/2012GL053421.
Neale, R., and J. Slingo (2003), The maritime continent and its role in the global climate: A GCM study, *J. Clim.*, *16*, 834–848.
Neelin, J. D., et al. (1992), Tropical air-sea interaction in general circulation models, *Clim. Dyn.*, *7*, 73–104.
Pearson, K. J., G. M. S. Lister, C. E. Birch, R. P. Allan, R. J. Hogan, and S. J. Woolnough (2014), Modelling the diurnal cycle of tropical convection across the 'grey zone', *Q. J. R. Meteorol. Soc.*, *140*, 491–499, doi:10.1002/qj.2145.
Pincus, R., S. Platnick, S. A. Ackerman, R. S. Hemler, and R. J. P. Hofmann (2012), Reconciling simulated and observed views of clouds: MODIS, ISCCP, and the limits of instrument simulators, *J. Clim.*, *25*, 4699–4720.
Potter, G. L., and R. D. Cess (2004), Testing the impact of clouds on the radiation budgets of 19 atmospheric general circulation models, *J. Geophys. Res.*, *109*, D02106, doi:10.1029/2003JD004018.
Raddatz, T. J., C. H. Reick, W. Knorr, J. Kattge, E. Roeckner, R. Schnur, K.-G. Schnitzler, P. Wetzel, and J. Jungclaus (2007), Will the tropical land biosphere dominate the climate-carbon cycle feedback during the twenty first century?, *Clim. Dyn.*, *29*, 565–574.
Rienecker, M. M., et al. (2011), MERRA—NASA's Modern-Era Retrospective Analysis for Research and Applications, *J. Clim.*, *24*, 3624–3648.
Rose, F. G., D. A. Rutan, T. P. Charlock, G. L. Smith, and S. Kato (2013), An algorithm for the constraining of radiative transfer calculations to CERES-observed broadband top-of-atmosphere irradiance, *J. Atmos. Oceanic Technol.*, *30*, 1091–1106.
Rossow, W. B., and R. A. Schiffer (1999), Advances in understanding clouds from ISCCP, *Bull. Am. Meteorol. Soc.*, *80*, 2261–2287.
Rutan, D., F. Rose, M. Roman, N. Manalo-Smith, C. Schaaf, and T. Charlock (2009), Development and assessment of broadband surface albedo from Clouds and the Earth's Radiant Energy System clouds and radiation swath data product, *J. Geophys. Res.*, *114*, D08125, doi:10.1029/2008JD010669.
Sato, T., H. Miura, M. Satoh, Y. N. Takayabu, and Y. Wang (2009), Diurnal cycle of precipitation in the tropics simulated in a global cloud-resolving model, *J. Clim.*, *22*, 4809–4826.
Slingo, A., K. I. Hodges, and G. J. Robinson (2004), Simulation of the diurnal cycle in a climate model and its evaluation using data from Meteosat 7, *Q. J. R. Meteorol. Soc.*, *130*, 1449–1467.
Soden, B. J., A. J. Broccoli, and R. S. Hemler (2004), On the use of cloud forcing to estimate cloud feedback, *J. Clim.*, *17*, 3661–3665.
Stratton, R. A., and A. J. Stirling (2012), Improving the diurnal cycle of convection in GCMs, *Q. J. R. Meteorol. Soc.*, *138*, 1121–1134.
Su, H., and J. H. Jiang (2013), Tropical clouds and circulation changes during the 2006/07 and 2009/10 El Niños, *J. Clim.*, *26*, 399–413.
Su, H., et al. (2012), Diagnosis of regime-dependent cloud simulation errors in CMIP5 models using "A-Train" satellite observations and reanalysis data, *J. Geophys. Res.*, 2762–2780, doi:10.1029/2012JD018575.

Su, W., A. Bodas-Salcedo, K.-M. Xu, and T. P. Charlock (2010), Comparison of the tropical radiative flux and cloud radiative effect profiles in a climate model with Clouds and the Earth's Radiant Energy System (CERES) data, *J. Geophys. Res.*, *115*, D01105, doi:10.1029/2009JD012490.

Sun, M., R. D. Cess, and D. R. Doelling (2012), Interpretation of cloud structure anomalies over the tropical Pacific during the 1997/98 El Niño, *J. Geophys. Res.*, *117*, D16114, doi:10.1029/2011JD015861.

Voldoire, A., et al. (2012), The CNRM-CM5.1 global climate model: Description and basic evaluation, *Clim. Dyn.*, *40*, 2091–2121, doi:10.1007/s00382-011-1259-y.

von Salzen, J., et al. (2012), The Canadian Fourth Generation Atmospheric Global Climate Model (CanAM4). Part I: Representation of physical processes, *Atmos. Ocean.*, *51*, 104–125.

Wang, B., L. Zhou, and K. Hamilton (2007), Effect of convective entrainment/detrainment on the simulation of the tropical precipitation diurnal cycle, *Mon. Weather Rev.*, *135*, 567–585.

Wang, H., and W. Su (2013), Evaluating and understanding top of the atmosphere cloud radiative effects in Intergovernmental Panel on Climate Change (IPCC) Fifth Assessment Report (AR5) Coupled Model Intercomparison Project Phase 5 (CMIP5) models using satellite observations, *J. Geophys. Res. Atmos.*, *118*, 683–699, doi:10.1029/2012JD018619.

Watanabe, M., et al. (2010), Improved climate simulation by MIROC5: Mean states, variability, and climate sensitivity, *J. Clim.*, *23*, 6312–6335.

Webb, M. J., C. Senior, S. Bony, and J.-J. Morcrette (2001), Combining ERBE and ISCCP data to assess clouds in the Hadley Centre ECMWF and LMD atmospheric climate models, *Clim. Dyn.*, *17*, 905–922.

Wolter, K., and M. S. Timlin (2011), El Niño/Southern Oscillation behaviour since 1871 as diagnosed in an extended multivariate ENSO index (MEI.ext), *Int. J. Climatol.*, *31*, 1074–1087.

Zelinka, M. D., S. A. Klein, and D. L. Hartmann (2012a), Computing and partitioning cloud feedbacks using cloud property histograms. Part I: Cloud radiative kernels, *J. Clim.*, *25*, 3715–3735.

Zelinka, M. D., S. A. Klein, and D. L. Hartmann (2012b), Computing and partitioning cloud feedbacks using cloud property histograms. Part II: Attribution to changes in cloud amount, altitude, and optical depth, *J. Clim.*, *25*, 3736–3754.

Zelinka, M. D., S. A. Klein, K. E. Taylor, T. Andrews, M. J. Webb, J. M. Gregory, and P. M. Forster (2013), Contributions of different cloud types to feedbacks and rapid adjustments in CMIP5, *J. Clim.*, *26*, 5007–5027, doi:10.1175/JCLI-D-12-00555.1.

Zhang, M. H., R. D. Cess, T. Y. Kwon, and M. H. Chen (1994), Approaches of comparison for clear-sky radiative fluxes from general circulation models with Earth Radiation Budget Experiment data, *J. Geophys. Res.*, *99*, 5515–5523, doi:10.1029/93JD03341.

Zhang, Y., S. Xie, C. Covey, D. D. Lucas, P. Gleckler, S. A. Klein, J. Tannahill, C. Doutriaux, and R. Klein (2012), Regional assessment of the parameter-dependent performance of CAM4 in simulating tropical clouds, *Geophys. Res. Lett.*, *39*, L14708, doi:10.1029/2012GL052184.